tion to digest adhesive proteins that were degraded and precipitated. Collected particles underwent sequential filtrations as previously reported.[22] The size of particles was defined as the maximum dimensions by the SEM analysis.

We compared the means of CLPE and MPC-CLPE groups by analysis of variance and determined significance by post-hoc testing using Bonferroni's method.

RESULTS

The XPS signals indicating nitrogen atoms (N_{1s}) at 402 eV and phosphorus atoms (P_{2p}) at 135 eV, which are attributable to the phosphorylcholine group in the MPC unit, were observed on the MPC-CLPE plate after gamma irritation (Fig 2A). The FTIR transmittance absorption representing phosphate group (P-O) at 1240, 1080, and 970 cm^{-1}, and ketone group (C = O) at 1720 cm^{-1} also was observed after grafting and irradiation (Fig 2B). The contact angle of a water droplet on the MPC-CLPE plate was 12.3° ± 2.4°, whereas the contact angle of a water droplet of the original cross-linked PE plate was 89.9° ± 2.9° (Fig 2C), suggesting the hydrophobic cross-linked PE surface was kept covered with hydrophilic MPC polymer after the gamma irritation.

In the hip simulator study (Fig 3A) the average friction torque was approximately 80% lower in MPC-CLPE liners than in cross-linked PE liners (Fig 3B). The gravimetric analysis showed a total weight loss of 34.7 ± 2.5 mg in cross-linked PE liners after 1×10^7 cycles of loading (Fig 3C). In contrast, MPC-CLPE liners continued to gain weight, showing a total weight gain of 8.7 ± 1 mg, which may have been attributable to water absorption into the liner from the lubricant.

Three-dimensional morphometric analyses of MPC-CLPE liner surface revealed little or no detectable wear, while substantial wear was detected in cross-linked PE liners (Fig 4A). The confocal scanning laser microscopic analysis of the liner surface clearly revealed original machine marks on the MPC-CLPE liner surface, but they were completely obliterated from the cross-linked PE liner (Fig 4B). The XPS analysis also confirmed the remainder of the specific spectra of N_{1s} and P_{2p} on the MPC-CLPE liner surface after the loading (Fig 2A), indicating the MPC-CLPE grafting was maintained after loading 1×10^7 cycles. The femoral heads were free of visible scratches and the surface roughness expressed by the R_a values was similar before and after loading in both groups (R_a = 0.04 – 0.05 μm), suggesting there was no abrasive contamination with metal particles from the heads in the hip simulator (Fig 4C).

The SEM analysis of the wear particles isolated from the lubricants showed no difference in the particle shapes or sizes between cross-linked PE and MPC-CLPE liners. Most of the particles from both liners ranged from 0.1 μm to1 μm and were round or spindle-shaped (Fig 5).

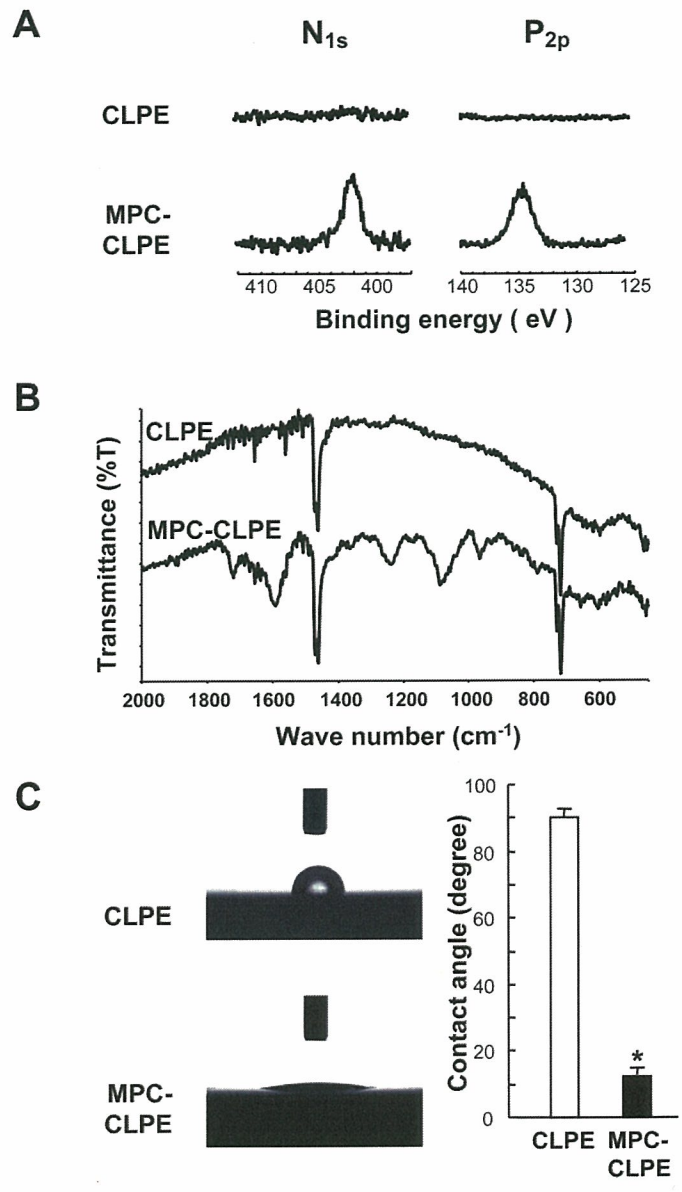

Fig 2A–C. (A) Xray photoelectron spectra of the cross-linked PE and MPC-CLPE plates after gamma sterilization are shown. The peaks in the nitrogen (N1s) and phosphorus (P2p) atom regions are specific to MPC, suggesting gamma sterilization did not affect the properties of MPC grafting. (B) Fourier transform infrared spectra of the cross-linked PE and MPC-CLPE plates after gamma sterilization are shown. Absorptions representing the phosphate group (P–O) at 1240, 1080, and 970 cm^{-1}, and ketone group (C = O) at 1720 cm^{-1} are also specific to MPC. (C) Hydrophilicity determined by the contact angle of a water drop with the cross-linked PE and MPC-CLPE plates after gamma sterilization is represented. Data are expressed as means (bars) ± standard errors (error bars) for 12 plates per group (*significant difference from cross-linked PE was set at $p < 0.01$).

Copyright © Lippincott Williams & Wilkins. Unauthorized reproduction of this article is prohibited.

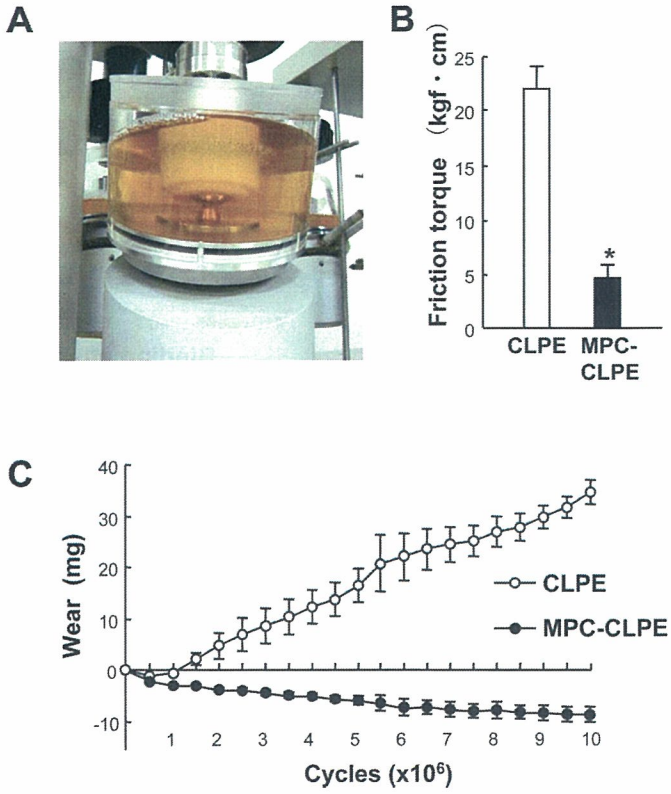

Fig 3A–C. (A) A photograph shows the hip simulator. (B) The bar graph shows friction torque of the cross-linked PE and MPC-CLPE liners against the femoral heads measured before the loading test. (C) The graph shows the time course of the amount of wear product from cross-linked PE and MPC-CLPE liners during 1×10^7 cycles of loading. Data are expressed as means (symbols and bars) ± standard errors (error bars) for 10 liners/group (*significant difference from cross-linked PE was set at $p < 0.01$).

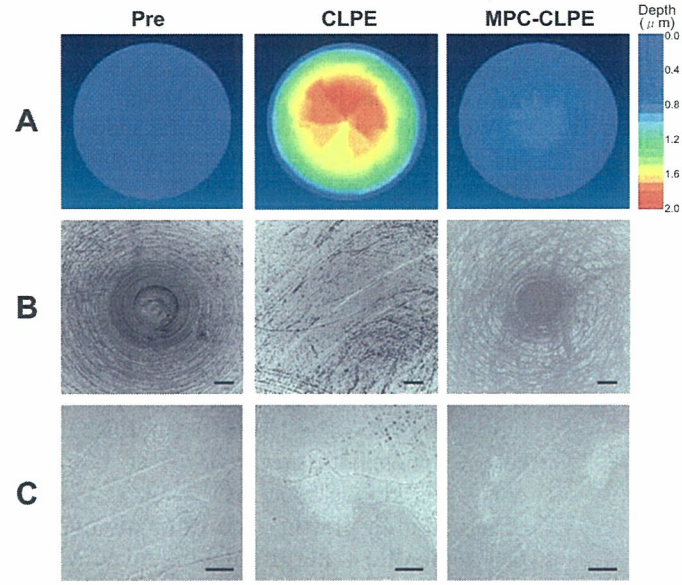

Fig 4A–C. (A) Three-dimensional morphometric analysis and (B) confocal scanning laser microscopic analysis of the liner surfaces before (pre) and after 1×10^7 cycles of loading on cross-linked PE and MPC-CLPE liners is shown (scale bars, 200 μm). (C) Scanning electron microscopy analyses of the femoral head surfaces before (pre) and after 1×10^7 cycles of loading showed the femoral heads were free of visible scratches in both liners (scale bars, 5 μm).

DISCUSSION

Our data suggest the biocompatible phospholipid polymer MPC grafted onto the PE liner surface of the hip prosthesis decreases friction and the production of wear particles during 1×10^7 cycles of loading in a hip simulator. Because PE particles are the most abundant and catabolic among wear particles in the periprosthetic tissues,[30] alternative bearing surfaces have been proposed such as ceramic-on-ceramic and metal-on-metal articulations; however, these have potential disadvantages.[2,3]

The major limitation of our study is the confined period of loading. Although the 1×10^7 cycles in the hip simulator is comparable to 10 to 30 years of physical walking, this may not be long enough for young active patients with aseptic necrosis or fracture. A hip simulator study with longer loading is now underway. Furthermore, a hip simulator does not entirely capture the range of loading conditions of a hip, in terms of either the variety of positions or the magnitude of loading. Nonetheless, we believe a simulator study can provide some indication of trends.

The long history and popularity of PE as a bearing surface has led to research in the development of tougher

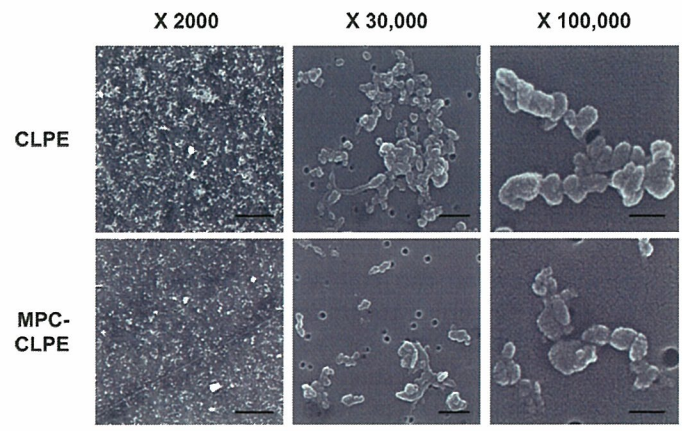

Fig 5. Scanning electron microscopy images show the wear particles isolated from lubricants of the simulators with cross-linked PE and MPC liners. Representative images are shown in three magnifications (×2000, ×30,000, and ×100,000; scale bars, 10 μm, 500 nm, and 200 nm, respectively).

Copyright © Lippincott Williams & Wilkins. Unauthorized reproduction of this article is prohibited.

and more wear-resistant PE materials. These include the incorporation of short chopped carbon fibers in PE matrix,[6,41] the extension of chain crystallite morphology with thicker lamellae and higher crystallinity,[28] and the creation of a three-dimensional molecular network by cross-linking. Of these, cross-linking improved the wear resistance and suppressed the periprosthetic osteolysis most efficiently in the clinical setting.[31] Grafting of MPC onto the cross-linked PE surface further increased the wear resistance over the conventional cross-linked PE.

Clinical and laboratory research suggests sterilization methods can dramatically affect the in vivo performance of PE liners.[32] Currently, PE liners can be sterilized with gamma irradiation, gas plasma, or ethylene oxide. Gamma sterilization in air has been shown to lead to oxidation of the PE and may adversely affect its mechanical properties. In the mid-1990s, the use of gamma sterilization in air was replaced by gamma sterilization in an inert environment, such as nitrogen, argon, or a vacuum. We used cross-linked PE liners sterilized gamma irradiation in nitrogen, and our data suggest this sterilization method did not affect the property of MPC grafting with respect to surface analysis and hip simulator study. Other MPC-grafted medical devices such as an oxygenator, intravascular stents, or intravascular guide wires are sterilized with gamma irradiation or ethylene oxide. Moreover, the MPC polymer has good thermal resistance and could be processed by heat treatment at 150°C. Our preliminary study showed gas plasma and ethylene oxide sterilization did not affect properties of the MPC polymer.[36]

Given a reduction of wear by the MPC grafting, we should consider the lubrication mechanism between the liners and metal heads. Although phospholipids work as effective boundary lubricants,[12,40] a study of natural synovial joints showed fluid film lubrication by the intermediate hydrated layer is the predominant mechanism under physiologic walking conditions.[7] Because we showed the MPC grafting onto the cross-linked PE plate increased hydrophilicity, and our previous study showed the free water fraction on the MPC polymer surface is kept at a higher level,[17] the reduction of wear is likely attributable to the hydrated lubricating layer formed by MPC grafting.

In addition to the improvement of the wear resistance of the liner, it is important to decrease bone resorptive responses induced by wear particles. Substantial differences between the wear particles from cross-linked and non-cross-linked PE liners have been found in vitro.[8,15] The cross-linked PE liner releases a relatively high number of submicrometer and nanometer-sized PE particles and relatively fewer particles that are several micrometers in dimension.[11] These submicrometer-sized PE particles induce a greater inflammatory response in vitro than larger particles.[15] Therefore, the biological activity of PE particles will depend on the total volume of wear or the number of particles generated and the proportion of those particles that are within the most biologically active size range.[8,11] In our previous study, MPC nanoparticles (500 nm in diameter) were used in a murine particle-induced osteolysis model to investigate the biocompatibility of these particles.[34] In vitro culture systems suggested MPC nanoparticles were not phagocytosed in substantial amounts by macrophages and do not induce the production of bone resorptive cytokines. Furthermore, the culture medium of macrophages exposed to MPC nanoparticles did not induce osteoclast formation from bone marrow cells. These results suggest MPC particles are biologically inert in respect to phagocytosis by macrophages and subsequent bone resorptive actions. An increasing number of studies address the potential pharmacologic modification of the adverse host response to wear particles,[5,10] including cytokine antagonists, cyclooxygenase-2 inhibitors, and osteoprotegerin, or anti-RANKL (receptor activator of nuclear vector kappa B ligand) antibody; however, they may cause serious side effects because the agents must taken for a long period after surgery and because they are not currently targeted to the site of the problem. Because the lack of side effects of the MPC polymer grafting has already been confirmed clinically by several biomaterials,[23,26] this grafting surpasses the developing pharmacologic treatments.

Although our study focused on the hip, MPC polymer grafting can be applicable to the prevention of periprosthetic osteolysis of other joints in which PE particles from articular interfaces between the PE and metal components are also thought to initiate the catabolic cascade.[14,39] From the advantages observed, we believe MPC polymer grafting will improve total joint replacement by preventing periprosthetic osteolysis and aseptic loosening. The development of this nanotechnology would improve the quality of care of patients having total joint replacement and have a substantial public health impact. We are currently designing a large-scale clinical trial.

Acknowledgments

We thank Tomohiro Konno, Noboru Yamawaki, Takatoshi Miyashita, Masayuki Kyomoto, Hiroaki Takadama, Kaori Jono, and Reiko Yamaguchi for their excellent technical help.

References

1. Birrell F, Johnell O, Silman A. Projecting the need for hip replacement over the next three decades: influence of changing demography and threshold for surgery. *Ann Rheum Dis*. 1999;58:569–572.
2. Black J. Metal on metal bearings. A practical alternative to metal on polyethylene total joints? *Clin Orthop Relat Res*. 1996;329: S244–S255.
3. Callaway GH, Flynn W, Ranawat CS, Sculco TP. Fracture of the femoral head after ceramic-on-polyethylene total hip arthroplasty. *J Arthroplasty*. 1995;10:855–859.

Copyright © Lippincott Williams & Wilkins. Unauthorized reproduction of this article is prohibited.

4. Charnley J. Total hip replacement by low-friction arthroplasty. *Clin Orthop Relat Res.* 1970:72:7–21.
5. Childs LM, Paschalis EP, Xing L, Dougall WC, Anderson D, Boskey AL, Puzas JE, Rosier RN, O'Keefe RJ, Boyce BF, Schwarz EM. In vivo RANK signaling blockade using the receptor activator of NF-kappaB:Fc effectively prevents and ameliorates wear debris-induced osteolysis via osteoclast depletion without inhibiting osteogenesis. *J Bone Miner Res.* 2002;17:192–199.
6. Connelly GM, Rimnac CM, Wright TM, Hertzberg RW, Manson JA. Fatigue crack propagation behavior of ultrahigh molecular weight polyethylene. *J Orthop Res.* 1984;2:119–125.
7. Dowson D, Jin ZM. Micro-elastohydrodynamic lubrication of synovial joints. *Eng Med.* 1986:15:63–65.
8. Galvin AL, Tipper JL, Ingham E, Fisher J. Nanometre size wear debris generated from crosslinked and non-crosslinked ultra high molecular weight polyethylene in artificial joints. *Wear.* 2005;259: 977–983.
9. Glant TT, Jacobs JJ, Molnar G, Shanbhag AS, Valyon M, Galante JO. Bone resorption activity of particulate-stimulated macrophages. *J Bone Miner Res.* 1993:8:1071–1079.
10. Goater JJ, O'Keefe RJ, Rosier RN, Puzas JE, Schwarz EM. Efficacy of ex vivo OPG gene therapy in preventing wear debris induced osteolysis. *J Orthop Res.* 2002:20:169–173.
11. Green TR, Fisher J, Stone M, Wroblewski BM, Ingham E. Polyethylene particles of a 'critical size' are necessary for the induction of cytokines by macrophages in vitro. *Biomaterials.* 1998;19: 2297–2302.
12. Hills BA. Boundary lubrication in vivo. *Proc Inst Mech Eng [H].* 2000:214:83–94.
13. Hills BA, Butler BD. Surfactants identified in synovial fluid and their ability to act as boundary lubricants. *Ann Rheum Dis.* 1984; 43:641–648.
14. Inagaki K, O'Driscoll SW, Neale PG, Uchiyama E, Morrey BF, An KN. Importance of a radial head component in Sorbie unlinked total elbow arthroplasty. *Clin Orthop Relat Res.* 2002:400:123–131.
15. Ingram JH, Stone M, Fisher J, Ingham E. The influence of molecular weight, crosslinking and counterface roughness on TNF-alpha production by macrophages in response to ultra high molecular weight polyethylene particles. *Biomaterials.* 2004;25:3511–3522.
16. Ishihara K, Iwasaki Y, Ebihara S, Shindo Y, Nakabayashi N. Photoinduced graft polymerization of 2-methacryloyloxyethyl phosphorylcholine on polyethylene membrane surface for obtaining blood cell adhesion resistance. *Colloids Surf B Biointerfaces.* 2000; 18:325–335.
17. Ishihara K, Nomura H, Mihara T, Kurita K, Iwasaki Y, Nakabayashi N. Why do phospholipid polymers reduce protein adsorption? *J Biomed Mater Res.* 1998;39:323–330.
18. Ishihara K, Okazaki A, Negishi N, Shinohara I, Okano T, Kataoka K, Sakurai Y. Photo-induced change in wettability and binding ability of azoaromatic polymers. *J Appl Polym Sci.* 1982;27: 239–245.
19. Ishihara K, Shinozuka T, Hanazaki Y, Iwasaki Y, Nakabayashi N. Improvement of blood compatibility on cellulose hemodialysis membrane: IV. Phospholipid polymer bonded to the membrane surface. *J Biomater Sci Polym Ed.* 1999;10:271–282.
20. Ishihara K, Ueda T, Nakabayashi N. Preparation of phospholipid polymers and their properties as polymer hydrogel membrane. *Polym J.* 1990;22:355–360.
21. Jacobs JJ, Roebuck KA, Archibeck M, Hallab NJ, Glant TT. Osteolysis: basic science. *Clin Orthop Relat Res.* 2001;393:71–77.
22. Jono K, Takigawa Y, Takadama H, Mizuno M, Nakamura T. A multi-station hip joint simulator study and wear characterization of commercial hip endoprostheses. *Ceram Eng & Sci Proc.* 2003:24: 255–260.
23. Kihara S, Yamazaki K, Litwak KN, Litwak P, Kameneva MV, Ushiyama H, Tokuno T, Borzelleca DC, Umezu M, Tomioka J, Tagusari O, Akimoto T, Koyanag H, Kurosawa H, Kormos RL, Griffith BP. In vivo evaluation of a MPC polymer coated continuous flow left ventricular assist system. *Artif Organs.* 2003;27: 188–192.
24. Kirk TB, Wilson AS, Stachowiak GW. The morphology and composition of the superficial zone of mammalian articular cartilage. *J Orthop Rheumatol.* 1993:6:21–28.
25. Kurtz S, Mowat F, Ong K, Chan N, Lau E, Halpern M. Prevalence of primary and revision total hip and knee arthroplasty in the United States from 1990 through 2002. *J Bone Joint Surg.* 2005:87: 1487–1497.
26. Lewis AL, Furze JD, Small S, Robertson JD, Higgins BJ, Taylor S, Ricci DR. Long-term stability of a coronary stent coating post-implantation. *J Biomed Mater Res.* 2002;63:699–705.
27. Lewis AL, Tolhurst LA, Stratford PW. Analysis of a phosphorylcholine-based polymer coating on a coronary stent pre- and post-implantation. *Biomaterials.* 2002;23:1697–1706.
28. Livingston BJ, Chmell MJ, Spector M, Poss R. Complications of total hip arthroplasty associated with the use of an acetabular component with a Hylamer liner. *J Bone Joint Surg Am.* 1997:79: 1529–1538.
29. Mahomed NN, Barrett JA, Katz JN, Phillips CB, Losina E, Lew RA, Guadagnoli E, Harris WH, Poss R, Baron JA. Rates and outcomes of primary and revision total hip replacement in the United States medicare population. *J Bone Joint Surg Am.* 2003;85:27–32.
30. Maloney WJ, Smith RL, Schmalzried TP, Chiba J, Huene D, Rubash H. Isolation and characterization of wear particles generated in patients who have had failure of a hip arthroplasty without cement. *J Bone Joint Surg Am.* 1995:77:1301–1310.
31. McKellop H, Shen FW, DiMaio W, Lancaster JG. Wear of gamma-crosslinked polyethylene acetabular cups against roughened femoral balls. *Clin Orthop Relat Res.* 1999;369:73–82.
32. McKellop H, Shen FW, Lu B, Campbell P, Salovey R. Effect of sterilization method and other modifications on the wear resistance of acetabular cups made of ultra-high molecular weight polyethylene. A hip-simulator study. *J Bone Joint Surg Am.* 2000:82: 1708–1725.
33. Merx H, Dreinhofer K, Schrader P, Sturmer T, Puhl W, Gunther KP, Brenner H. International variation in hip replacement rates. *Ann Rheum Dis.* 2003;62:222–226.
34. Moro T, Takatori Y, Ishihara K, Konno T, Takigawa Y, Matsushita T, Chung UI, Nakamura K, Kawaguchi H. Surface grafting of artificial joints with a biocompatible polymer for preventing periprosthetic osteolysis. *Nat Mater.* 2004;3:829–836.
35. Muratoglu OK, Greenbaum ES, Bragdon CR, Jasty M, Freiberg AA, Harris WH. Surface analysis of early retrieved acetabular polyethylene liners: a comparison of conventional and highly crosslinked polyethylenes. *J Arthroplasty.* 2004:19:68–77.
36. Ogawa R, Iwasaki Y, Ishihara K. Thermal property and processability of elastomeric polymer alloy composed of segmented polyurethane and phospholipid polymer. *J Biomed Mater Res.* 2002;62: 214–221.
37. Older J. Charnley low-friction arthroplasty: a worldwide retrospective review at 15 to 20 years. *J Arthroplasty.* 2002:17:675–680.
38. Paul JP. Forces transmitted by joints in the human body. *Proc Inst Mech Eng [H].* 1967;181:8–15.
39. Shanbhag AS, Bailey HO, Hwang DS, Cha CW, Eror NG, Rubash HE. Quantitative analysis of ultrahigh molecular weight polyethylene (UHMWPE) wear debris associated with total knee replacements. *J Biomed Mater Res.* 2000;53:100–110.
40. Williams PF 3rd, Powell GL, LaBerge M. Sliding friction analysis of phosphatidylcholine as a boundary lubricant for articular cartilage. *Proc Inst Mech Eng [H].* 1993;207:59–66.
41. Wright TM, Rimnac CM, Faris PM, Bansal M. Analysis of surface damage in retrieved carbon fiber-reinforced and plain polyethylene tibial components from posterior stabilized total knee replacements. *J Bone Joint Surg Am.* 1988;70:1312–1319.
42. Yoneyama T, Sugihara K, Ishihara K, Iwasaki Y, Nakabayashi N. The vascular prosthesis without pseudointima prepared by antithrombogenic phospholipid polymer. *Biomaterials.* 2002;23: 1455–1459.

Copyright © Lippincott Williams & Wilkins. Unauthorized reproduction of this article is prohibited.

Available online at www.sciencedirect.com
SCIENCE DIRECT®
Biomaterials 27 (2006) 5151–5160
Biomaterials
www.elsevier.com/locate/biomaterials

Biomimetic phosphorylcholine polymer grafting from polydimethylsiloxane surface using photo-induced polymerization

Tatsuro Goda[a], Tomohiro Konno[a], Madoka Takai[a], Toru Moro[b], Kazuhiko Ishihara[a,*]

[a]*Department of Materials Engineering, School of Engineering and Center for NanoBio Integration, The University of Tokyo, 7-3-1, Hongo, Bunkyo-ku, Tokyo 113-8656, Japan*
[b]*Department of Orthopedic Surgery, Faculty of Medicine, The University of Tokyo, 7-3-1, Hongo, Bunkyo-ku, Tokyo 113-8656, Japan*

Received 24 February 2006; accepted 29 May 2006
Available online 23 June 2006

Abstract

The biomimetic synthetic phospholipid polymer containing a phosphorylcholine group, 2-methacryloyloxyethyl phosphorylcholine (MPC), has improved the surface property of biomaterials. Both hydrophilic and anti-biofouling surfaces were prepared on polydimethylsiloxane (PDMS) with MPC grafted by surface-initiated photo-induced radical polymerization. Benzophenone was used as the photoinitiator. The quantity of the adsorbed initiator on PDMS was determined by UV absorption and ellipsometry. The poly(MPC)-grafted PDMS surfaces were characterized by XPS, ATR-FTIR and static water contact angle (SCA) measurements. The SCA on PDMS decreased from 115° to 25° after the poly(MPC) grafting. The in vitro single protein adsorption on the poly(MPC)-grafted PDMS decreased 50–75% compared to the unmodified PDMS. The surface friction of the poly(MPC)-grafted PDMS was lower than the unmodified PDMS under wet conditions. The oxygen permeability of the poly(MPC)-grafted PDMS was as high as the unmodified PDMS. The tensile property of PDMS was maintained at about 90% of the ultimate stress and strain after the poly(MPC) grafting. The surface-modified PDMS is expected to be a novel medical elastomer which possesses an excellent surface hydrophilicity, anti-biofouling property, oxygen permeability and tensile property.
© 2006 Elsevier Ltd. All rights reserved.

Keyword: Polydimethylsiloxane; Phosphorylcholine; Protein adsorption; Wettability; Oxygen permeation; Friction

1. Introduction

Polydimethylsiloxane (PDMS)-based materials have been applied to various medical devices, such as ophthalmologic biomaterials, microfluidic devices, an artificial lung [1], and an artificial finger joint [2] due to its attractive properties of high oxygen permeability, good mechanical property, optical transparency, self-sealing property, convenient processability, and chemical stability. On the other hand, the native hydrophobicity and biofouling tendency of PDMS has been one of its biggest limitations for biomaterial applications. For example, nonspecific protein adsorption on a material is recognized as the first incident leading to subsequent events including thrombus formation, foreign body reaction, bacterial infection, and other undesirable responses. Owing the supersensitive analysis of microfluidic systems, the adsorption of biomolecules on PDMS significantly reduces the signal/noise ratio during detection [3]. As for an artificial lung, the blood activation on a large blood contact surface area is the critical problem [4]. Consequently, there are tremendous needs for methods to quickly and easily modify the surface properties of PDMS.

To modify the disadvantages of PDMS-based materials, oxygen plasma treatment is a simple and the most widespread technique to change its surface hydrophobicity [5–9]. However, the hydrophilic nature of oxidized PDMS is only temporary as the migration of PDMS chains leads to recovery of the native hydrophobic state [10–12]. Surface coating or grafting with hydrophilic polymers on PDMS is another technique [13]. Surface graft polymerization is better than coating due to the chemical stability of its covalent bonding with a substrate and lower risk for

*Corresponding author. Tel.: +81 3 5841 7124; fax: +81 3 5841 8647.
E-mail address: ishihara@mpc.t.u-tokyo.ac.jp (K. Ishihara).

0142-9612/$ - see front matter © 2006 Elsevier Ltd. All rights reserved.
doi:10.1016/j.biomaterials.2006.05.046

deposition. The grafting methods can be divided into two classifications known as "grafting-to" and "grafting-from" [14]. For the "grafting-to" method, the polymer chains carrying reactive anchor groups at the end or the side chains are covalently coupled to the PDMS surface using silane-coupling reagents. Plasma treatment can also introduce active species on a surface of the polymer, followed by polymerization of the monomers. However, the complication inherent in the "grafting-to" process is an intrinsic limitation of the number of functional groups per surface area for thermodynamic reasons [15]. On the other hand, the "grafting-from" method utilizes active species existing on a polymer surface with a high grafting density to initiate the polymerization of monomers from the surface. "Grafting from" can be usually accomplished by treating a substrate with plasma and glow-discharge to generate the immobilized initiators followed by polymerization [16]. However, immobilization of the initiator on the surface involves several steps that may lead to low graft densities of the initiator and tethered polymer if the reactions are not quantitative. In addition, a side reaction, which possibly exists in the initiator immobilization reaction, may introduce some undesired structures on the surface. Methods that circumvented these problems have also been reported to accurately attach initiators in one step on the surface of the substrate using self-assembly monolayer techniques [17]. Accurate characterization of the initiator is important for the "grafting-from" method. Recently, living polymerization techniques have extensively been investigated in order to grow high-density polymer brushes with a controlled length and narrow molecular weight distribution. Atom transfer radical polymerization (ATRP) is useful because of its versatility including monomer types, tolerance of impurities, and mild reaction conditions [18,19]. Although the ATRP grafting technique onto PDMS surfaces seems attractive for biomaterials, a simple scheme is preferable for practical use [20].

Selection of the grafting polymer is the next parameter. Various types of polymers, such as poly(ethylene oxide) (PEO), poly(2-hydroxyethyl methacrylate), poly(2-hydroxyethyl acrylate), poly(acrylic acid), poly(acrylamide), and poly(*N,N*-dimethylacrylamide) were grafted onto the PDMS surfaces to make ideal biomaterial surfaces. Among these monomers, the PEO grafted surface has shown good anti-biofouling characteristics. The use of biomimetic materials is another promising approach to enhance the anti-fouling property and biocompatibility. The biomembrane-mimetic surface based on phosphorylcholine containing phospholipid polymers have shown an excellent resistivity of non-specific protein adsorption and cell adhesion [21–27]. These biomimetic polymers are included in 2-methacryloxloxyethyl phosphorylcholine (MPC), a methacrylate monomer having a zwitterionic phosphorylcholine headgroup in the side chain [28]. Poly(MPC) is known to possess a large amount of the free water fraction around the chain, which resists non-specific protein adsorption, and this also provides stabilization of biomolecules such as enzymes and proteins, even when the biomolecules are adsorbed on the surface [29–31].

In this paper, we reported the MPC "grafting-from" polymerization on PDMS using UV light. This polymerization has advantages in simplicity and efficiency. A graft polymerization was conducted in the MPC aqueous solution. This process made benzophenone remain on the PDMS surface after being placed in the monomer solution because benzophenone is insoluble in water. Therefore, the "grafting-from" polymerization can be performed on the surface attached benzophenone. The use of UV light to initiate a chemical reaction is applicable for the photolithographic micropatterning and the generation of multifunctional patterns at selected areas of the substrate. A similar poly(MPC) grafting was reported on an ultrahigh-molecular-weight polyethylene surface to decrease the friction and the amount of wear, and to improve the biocompatibility for an artificial hip joint [32,33]. Meanwhile, the main objective of the current study is to obtain a novel medical elastomer possessing a surface hydrophilicity, non-biofouling property, lubrication property, high-oxygen permeability and elasticity. Also, we checked the tensile properties of the poly(MPC)-grafted PDMS because the radicals may affect the elasticity of PDMS due to the formation of cross-links.

2. Experimental section

2.1. Materials

MPC was synthesized by a previously described method [28] and recrystallized from acetonitrile. Bovine serum albumin, bovine serum γ-globulin, and bovine plasma fibrinogen were purchased from Sigma-Aldrich Japan, and lysozyme from chicken egg white was purchased from Biozyme (Blaenavon, UK). The precursor of PDMS (Silpot 184®) and cross-linker of PDMS (Catalyst of Silpot 184®) were purchased from Toray-Dow Corning Co. (Tokyo, Japan). All other reagents and solvents were commercially available as extra-pure grade and were used as purchased. Distilled water was used in all the experiments. The nitrogen, oxygen, and argon gases were of high-purity grade.

2.2. Preparation of PDMS

The precursor of PDMS and cross-linker were fully mixed at the ratio of 10:1 by mass. The mixtures (5 mL) were evenly spread on a glass plate (10 cm × 10 cm) and degassed in a vacuum oven for 2 h at 25 °C. The curing reaction was then carried out at 60 °C for 6 h. The samples were cut into disks (10 mm diameter, 0.5 mm thickness) or the desired shapes.

2.3. Preparation of poly(MPC)-grafted PDMS

The PDMS was etched by oxygen plasma (300 W, 100 mL/min gas flow) for 1 min in advance. The MPC graft polymerization was able to be completed without the plasma treatment. The membrane was immersed in a 30 mL acetone solution containing benzophenone for 1 min. In the feed benzophenone concentration, "*x*", was varied from 0.1 to 10 g/L. The membrane was dried in vacuo under dark condition for 1 h at 25 °C. The concentration of the MPC aqueous solution, "*y*" (= 0.25 or 0.50 mol/L), was prepared in degassed pure water and then argon was bubbled for 3 min to eliminate any oxygen. As the sample nomenclature, the surface modified PDMS membranes are coded by "*x*–*y*" using a simplified

numerical value of the initiator and monomer concentrations in the feed. The benzophenone coated PDMS was set between the slide glasses filled with the MPC monomer solution. The amount of the MPC solution between the PDMS and slide glasses was 10 μL/cm^2. The photo polymerization on the PDMS surface was carried out using a 500 W ultra-high pressure mercury lamp (UVL-400HB, Riko Co, Chiba, Japan) at a distance of 10 cm for 120 min at 30 °C without using an optical filter. After the reaction, the membrane was successively washed in water and ethanol for 15 min and dried for 24 h at room temperature.

2.4. Amount of adsorbed initiator on PDMS

The amount of physically adsorbed benzophenone on the PDMS membrane was determined by ultraviolet absorption of the ethanol solution at 251 nm. The membrane was immersed in 5.0 mL of ethanol and ultrasonication was done for 60 min to detach the benzophenone from the PDMS membrane. The adsorbed initiator layer thickness on the PDMS membrane was checked by ellipsometry (DVA-36L3, Mizojiri Optical Co., Tokyo, Japan). The He–Ne laser (632.8 nm) entered at a 70° incident angle. The refractive index (n_r) of PDMS and benzophenone were applied at 1.414 and 1.598, and the extinction coefficients (k_e) were 0.010 and 0.000, respectively.

2.5. Surface characterization

XPS: The surface chemical composition was determined by X-ray photoelectron spectroscopy (XPS) using a magnesium anode non-monochromatic source (Kratos-Shimazu, Kanagawa, Japan). All samples were completely dried in vacuo before use. Survey scans (0–1100 eV) were performed to identify the C, O, N, P and Si elements. Takeoff angles of the photoelectrons were 90° and 20°. The data were collected at three locations on each sample. All binding energies were referenced the C1s peak at 285.0 eV. Their elemental compositions were determined by the peak areas corresponding to these elements.

ATR–FTIR: The measurement of the IR spectrum of the surface modified and unmodified PDMS membranes were carried out with an attenuated total reflection (ATR) apparatus spectrometer (FTIR-500, Jasco Co., Tokyo, Japan) under dry conditions. The spectra were recorded from 400 to 4000 cm^{-1} at a 4 cm^{-1} resolution. A single beam reference spectrum of a freshly cleaned ZnSe crystal at an incident angle of 45° was recorded before the measurements and used as the background spectrum.

Ellipsometry: The thickness of the poly(MPC) graft layers on the PDMS under dry condition was determined by ellipsometry (DVA-36L3, Mizojiri Optical Co., Tokyo, Japan). The He–Ne laser (632.8 nm) at a 70° incident angle was performed. The n_r and k_e of poly(MPC) are 1.488 and 0.000, respectively. All measurements were conducted in air at room temperature. The data were collected at nine locations for each sample.

SEM: Scanning electronic microscopy (SEM) was performed for obtaining the cross-sectional images of the modified and unmodified PDMS membranes using a SM-200 scanning microscope (Topcon Co, Tokyo, Japan) at an acceleration voltage of 15 keV. After the PDMS membranes were gently torn, the cross-sectional areas were coated with gold using a sputter (IB-3 ion coater, Eiko Engineering, Ibaraki, Japan).

Contact angle: The static water contact angles were measured using a goniometer (Kyowa Interface Science Co., Tokyo, Japan) at room temperature. The samples were dried in vacuo for 24 h before the measurements. Water droplets of 6 μL were contacted onto the membrane and the contact angles at 10 s were directly measured by photographic images. The data were collected at 10 positions on each sample.

AFM: The surface morphological AFM images in air and in water were checked using a NanoScope IIIa Multimode AFM (Nippon Veeco Co., Tokyo, Japan) in the tapping mode. For the measurements in air, anisotropic silicon probes with a height of 15–20 μm mounted on a rectangular beam with a spring constant of 40 N/m and a resonance frequency of about 210–250 kHz were used. A fluid cell (Nippon Veeco Co., Tokyo, Japan) was used for the measurements in water. Square pyramidal silicon nitride tips with a height of 2.5–3.5 μm mounted on a triangular silicone nitride cantilever with a spring constant of 0.12 N/m were used. The excitation frequency used in the fluid tapping was about 5–9 kHz and the drive amplitude was 700 mV. The scan rate was 1 Hz and the scan size was 25 μm × 25 μm for each sample. The root mean square (RMS) roughness at 25 μm × 25 μm was evaluated using bundled software.

2.6. Protein adsorption

In vitro single protein adsorption experiments were performed in phosphate-buffered saline (PBS, pH = 7.4, 0.15 mol/L) [34]. Samples were immersed in 4.5 mg/mL of bovine serum albumin, 1.6 mg/mL of γ-globulin from bovine blood, 0.3 mg/mL of fibrinogen from bovine serum, and 2.0 mg/mL of lysozyme from chicken egg white solutions, respectively. Clean, modified and unmodified PDMS membranes were first immersed in PBS filled 24-well plate for 24 h in order to be full hydrated. The specimens were moved into wells containing single protein solutions, and adsorptions were allowed to proceed at 37 °C for 2 h under gentle shaking. Each sample was then rinsed in the fresh PBS by 50 dippings. The samples were subsequently transferred into a well-plate filled in 1 mL of PBS solution containing 1 wt% of sodium dodecyl sulfate (SDS), and the surface adsorbed protein was completely desorbed by sonication for 20 min. A protein analysis kit (Micro BCA^{TM} protein assay reagent kit, #23235, Pierece, Rockford, IL, USA) based on the bicinchoninic acid (BCA) method was used to determine the concentration of the protein in the 1 wt% SDS solution. The amount of protein on the poly(MPC)-grafted PDMS was calculated from the concentration in the SDS solution. The concentration of the protein was measured by an absorptiometer (Wallac 1420 ARVO sx, Perkin-Elmer, Japan) at 560 nm.

2.7. Friction test

The surface frictional coefficients during start-up and under steady state conditions were measured using a tribo-tester (Heidon type32, Shinto Science Co., Tokyo, Japan). Sample membranes were cut into rectangular shapes (25 mm × 45 mm) and then completely wet by water or PBS (0.1 mol/L) before and during the measurements. The measurements were conducted by sliding the membrane under a 50 g load using a stainless-steel disk (25 mm in diameter). The scan speed and scale were 10 mm/s and 20 mm, respectively.

2.8. Oxygen permeability

The determination of the oxygen permeability of the PDMS membrane was performed by an electrochemical method. The polarographic cell was a cylindrical cathode of platinum coated by a resin on the side of cylinder (3 mm inner diameter, 6 mm outer diameter, and 40 mm length), and a wire anode of silver (10 mm length). The electrodes were connected to a potentiometer (HA 150 G, Hokuto Denko, Tokyo, Japan) to maintain the cathode at 0.7 V with respect to the anode. The water equilibrated PDMS membrane was cut into a disks (3 mm diameter, 0.5 mm thickness) and placed on the cathode. A piece of moistened filter paper (#N3KNA606, Millipore) punched into the same shape as the specimen was placed between the PDMS and the cathode to facilitate the transport of the electric current. The number of filter papers was changed from one to five in order to examine the effect of oxygen permeation at the boundary layer. The membrane was put in an acrylic ring plate so as not to allow oxygen to permeate the side of the membrane. The prepared cathode was covered then fastened with the small mesh. The electrodes were placed in the polarographic cell filled with 0.9 wt% of saline solution (1000 mL), whose temperature was controlled at 35 ± 0.1 °C by a thermostated water bath. The oxygen permeation was measured by performing a deoxygenation process of the membrane as follows: nitrogen was passed through the system thus producing the decrease in the electric current due to the consumption of the oxygen existing in the system. When the lowest current intensity was obtained, the nitrogen flow was stopped and pure oxygen at a pressure of 760 mmHg was bubbled into the system and allowed to reach

a steady-state condition. In all cases, the steady-state conditions were obtained in 20 min. The time dependent current change was monitored to obtain the diffusion coefficient. After the measurement, the sample was removed and the deoxygenation process reocurred to examine the current without the sample. A second piece of wet filter paper was then placed over the first one and the sample was repositioned on the top of the filter paper. The experiments were repeated until a total of five pieces of filter paper were used. In all cases, the residual current was measured in the deoxygenated system and subtracted from each current measurement.

The electrochemistry of oxygen permeation has been described in many papers [35,36]. For the mechanism used in this study, the oxygen permeates from one side of the membrane where the oxygen pressure is kept constant ($p_0 = 760$ mmHg) to the other side facing the cathode of the polarographic cell ($p_1 \approx 0$ mmHg). Under the steady-state during the driving force of a concentration gradient, oxygen diffuses across the membrane towards the cathode and the flux of oxygen can be expressed by Fick's first law by assuming Henry's law ($c = kp$, $\Delta p = p_0 - p_1$) as follows:

$$J = -D(\partial c/\partial x) = -Dk(\partial p/\partial x) \approx -Dk\,\Delta p/L_{x=L,t\to\infty}, \quad (1)$$

where D, c, k and L are, respectively, the diffusion coefficient, concentration, solubility coefficient and sample thickness. The equation can be applied to the electrochemical reactions at the electrodes where four electrons react with an oxygen molecule under the following conditions for the pressure $p(x, t)$:

$$p(0,0) = 0; \quad p(L,0) = 0; \quad p(0,t) = p0; \quad p(L,t) = 0, \quad (2)$$

$$I(t \to \infty) = -nFAJ = nFADk\Delta p/L, \quad (3)$$

where n is the number of electrons for the electrochemical reaction ($n = 4$), F is Faraday's constant (96,500 A s/22,400 cm^3 O_2 [STp]), and A is the surface area of the cathode (7.07×10^{-2} cm^2). The apparent oxygen transmittance is expressed by Eq. (3) as

$$Dk/L = I/nFA\,\Delta p = BI, \quad (4)$$

where B ($= (nFA\Delta p)^{-1} = 1.08 \times 10^{-3}$ (cm^3 O_2(STp)/cm^2/s mmHg)) is a constant under the given conditions. By considering that the inverse of the transmittance (L/Dk) is regarded as a resistance of permeation, the apparent resistance is divided by each resistance component (filter paper, boundary layer and membrane) and the law of resistors leads to

$$(L/Dk)_{app} = n(L/Dk)_{paper} + (L/Dk)_{BL} \quad (5)$$

for the experiments without membrane, and

$$(L/Dk)_{app} = n(L/Dk)_{paper} + (L/Dk)_{BL} + (L/Dk)_{membrane} \quad (6)$$

for the experiments with a membrane [37]. By plotting $(L/Dk)_{app}$ versus n (Eqs. (5) and (6)), determining the best fit by a least-squares analysis and extrapolating to zero layers of filter paper, $(L/Dk)_{BL}$ and $(L/Dk)_{membrane}$ are obtained. Dk was expressed in terms of barrer ($= 10^{-11}$ cm^3[STP] cm/s cm^2 mmHg).

2.9. Tensile test

The ultimate stress and strain of the poly(MPC)-grafted PDMS membranes were examined using a tensile tester (STA-1150, ORIENTEC, Tokyo, Japan). The samples were cut into a dumbbell shape (12.5 mm × 2.5 mm) at the thickness of 0.5 mm and strained at a 30 mm/min cross-head speed at room temperature. Each sample was examined five times.

3. Results and discussion

3.1. MPC graft polymerization on PDMS

Fig. 1 illustrates the MPC graft polymerization scheme on the PDMS surface. The grafting location can be restricted to the membrane surface. The benzophenone adsorbed on the substrate membrane exhibits a well-known photochemical reaction. The benzophenone is excited to the triplet state, which extracts a hydrogen atom from the α-methyl group of the substrate to produce polymer radicals capable of initiating graft polymerization of the monomers. The excited benzophenone finally changes to benzopinacol [38]. In this study, the dip coating procedure of benzophenone was applied using 0.1, 1.0, 5.0, and 10.0 g/L concentrations in an acetone solution. The amount of the physically adsorbed benzophenone on the PDMS membrane was determined by UV absorbance and ellipsometry. Fig. 2 shows the relationship between feed concentration of benzophenone, the adsorbed density of benzophenone, and the adsorbed thickness of benzophenone on the PDMS. The adsorbed density on the PDMS surface was saturated at $x \geqslant 5$ g/L, while the adsorbed thickness was constant (ca. 3.7 nm) at $x \geqslant 1$ g/L. The initiator density at $x = 1$ was about 30% of the saturated condition ($x \geqslant 5$ g/L) although its thickness was the same. These results indicate that the benzophenone roughly adsorbs on the PDMS at $x = 1$ with low feed

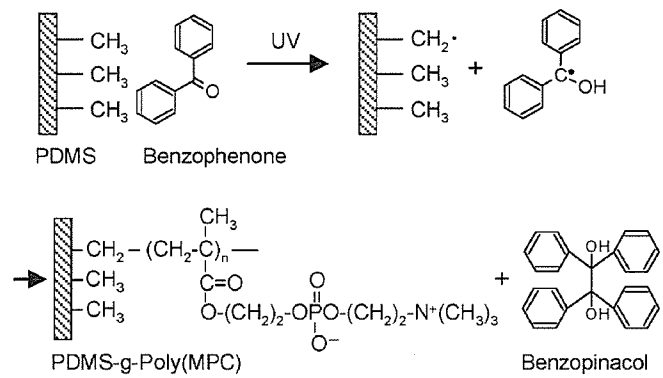

Fig. 1. Scheme of the UV-induced free radical surface graft polymerization onto a PDMS surface.

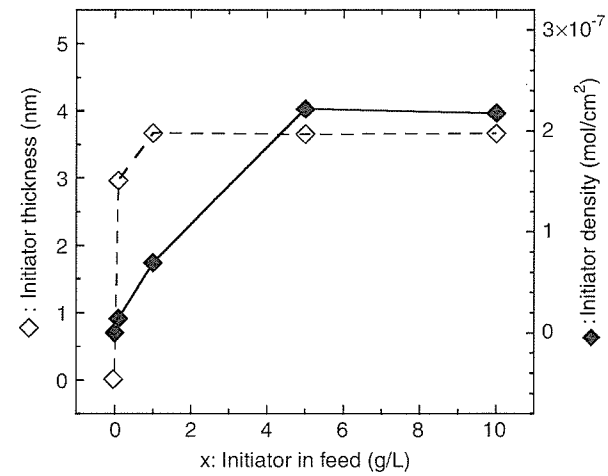

Fig. 2. Relationship between in feed initiator concentration and the amount of physically adsorbed initiator onto a PDMS surface.

concentration. It was also revealed that there was no difference in the amount of adsorption between $x = 5$ and 10. Fig. 3 shows the relationship of the UV irradiation time versus the static water contact angle (a) and graft layer thickness (b) for 10–0.25. The contact angles linearly decreased with an increase in the UV irradiation time. This was due to the increased graft layer thickness of the hydrophilic poly(MPC), and the ellipsometric data supported this result. The contact angles finally reached a constant at a specific UV irradiation time so that the irradiation was sufficient at 120 min for the MPC graft polymerization. This result implies that the crosslinks of the poly(MPC) graft chains or further polymerization are induced by the radicals. This is because the free radical graft polymerization is unable to control the chain length by the UV irradiation time. The detachment of the poly(MPC)-grafted on the PDMS was investigated. However, the poly(MPC) was not detected after the surface modified PDMS was washed in ethanol for 1 h.

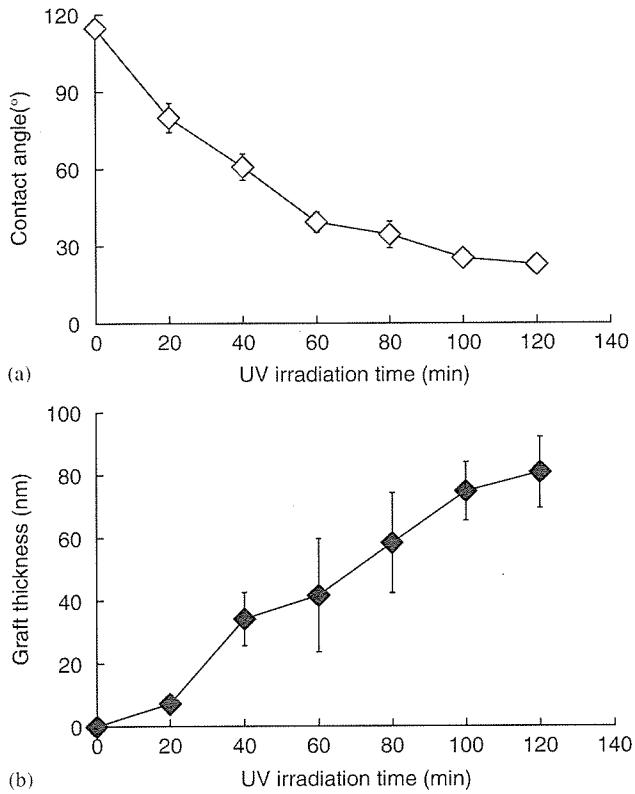

Fig. 3. Relationship between UV irradiation time during polymerization of 10–0.25 and static water contact angles on the poly(MPC)-grafted PDMS membranes (a), poly(MPC) graft layer thickness under dry condition (b).

3.2. Surface characterization

The poly(MPC)-grafted PDMS surfaces with different feed initiator and monomer concentrations were characterized. Based on the result shown in Fig. 3, the 120 min UV exposure time was selected for the poly(MPC) grafting on the PDMS surface. Table 1 shows the elemental compositions of poly(MPC)-grafted PDMS surfaces determined by XPS at the takeoff angles of 90° and 20°. The low-resolution XPS measures the uppermost surface elemental composition. The N and P compositions at the takeoff angle of 20° were lower than those at 90°, indicating that the hydrophilic phosphorylcholine groups were buried inside the PDMS, and the hydrophobic groups were at the outermost surface under the high vacuum condition. Among the 5–0.5, 10–0.5, 5–0.25, and 10–0.25, the N and P compositions were almost the same. These small differences in elemental compositions were in good agreement with the amount of adsorbed initiator. Their N and P compositions at the takeoff angle of 90° were slightly lower than the theoretical values of poly(MPC). The effects of the difference in monomer concentration were observed among the samples with a low initiator adsorption amount, such as 1–0.5 and 1–0.25. The experimental N/P ratios were lower than their theoretical value of 1.0. No N and P amounts were detected without the initiator condition (0–0.5).

Table 1
Surface elemental compositions of the poly(MPC)-grafted PDMS membranes with different initiator and monomer feed concentrations using XPS at a 90° and 20° takeoff angles

Sample	Take off angle 90° (Atom%)					Take off angle 20° (Atom%)				
	C	O	N	P	Si	C	O	N	P	Si
PDMS	46.1	30.8	0.0	0.0	23.1	46.6	28.4	0.0	0.0	25.0
0–0.5[a]	35.9	40.3	0.0	0.0	23.7	43.7	31.8	0.0	0.0	24.4
1–0.5	46.2	36.7	2.7	3.0	11.3	45.8	31.8	0.7	1.6	20.0
5–0.5	49.6	33.8	3.6	3.8	9.2	48.0	32.2	1.3	2.3	16.2
10–0.5	51.0	33.3	2.9	3.7	9.1	49.3	30.3	1.6	2.1	16.7
1–0.25	36.6	38.9	0.8	0.2	23.4	47.0	28.5	0.1	0.2	24.2
5–0.25	42.6	36.9	2.0	2.6	15.9	46.3	33.4	1.0	1.9	18.2
10–0.25	49.3	35.3	2.9	3.4	9.2	47.2	32.1	1.5	2.4	16.8
Poly(MPC)[b]	57.9	31.6	5.3	5.3	—	57.9	31.6	5.3	5.3	—

Data precision ~±3%.
[a]Without initiator adsorption in the graft polymerization.
[b]Theoretical composition of the poly(MPC).

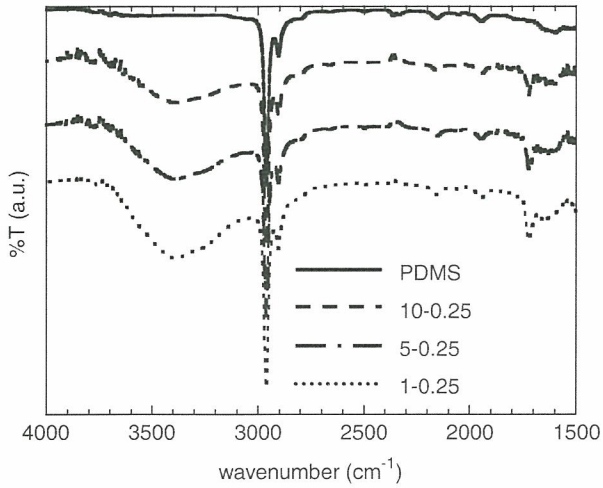

Fig. 4. ATR–FTIR spectra of poly(MPC)-grafted PDMS membranes with varying feed initiator concentration conditions during polymerization.

Fig. 4 shows the ATR–FTIR spectra of the poly(MPC)-grafted PDMS and unmodified PDMS under dry conditions. Among the poly(MPC)-grafted PDMS membranes, a new peak was observed at 1736 cm^{-1} which corresponded to the ester group in the poly(MPC). The hydroxyl group originated broad absorptions from 3000 to 3700 cm^{-1} were also observed for the poly(MPC)-modified PDMS due to the slight water uptake from the atmosphere into the poly(MPC) graft layer.

Fig. 5 shows the relationships between in feed initiator concentrations and static water contact angles on the poly(MPC) grafted PDMS (a), and poly(MPC) graft layer thicknesses determined by ellipsometry (b). In Fig. 5(a), the contact angles were drastically decreased from $x = 0$ to 1 and were almost constant at $x \geqslant 5$. This result strongly agrees with the amount of physically adsorbed initiator on the PDMS surface. In Fig. 5(b), the poly(MPC) graft layer thicknesses were almost constant. This also corresponded to the results from XPS and the water contact angles. The MPC monomer concentration was less important for the grafting than the amount of surface adsorbed initiator.

Fig. 6 shows the cross-sectional SEM images of the poly(MPC)-grafted PDMS (a), and the unmodified PDMS (b). In Fig. 6(a), the poly(MPC) graft layer can be directly seen as a white line on the edge between the PDMS and space. In addition, the thickness was determined to be about 80 nm. This result is a good agreement with the ellipsometric measurement.

The surface morphological images under dry and in-water conditions were studied using AFM. Fig. 7 shows the morphological images of the unmodified PDMS under dry (a), and PDMS in water (b), poly(MPC)-grafted PDMS (10–0.25) under dry (c), and 10–0.25 in water (d). The large domain of the poly(MPC)-grafted layer was observed on 10–0.25 under both conditions. The images in Fig. 7 show that the PDMS surfaces were completely covered with the poly(MPC) graft layers. The RMS roughness of 10–0.25

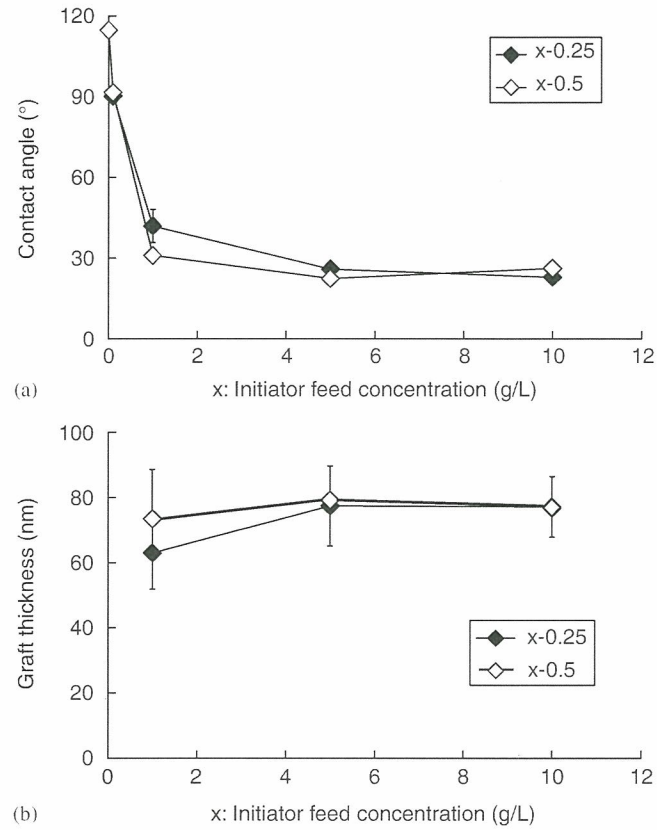

Fig. 5. Relationship between in feed initiator concentrations during polymerization and static water contact angles on the surface modified PDMS membrane (a), poly(MPC) graft layer thickness under dry condition (b).

under the dry condition was 61.0 nm, 290% higher than that in water (21.3 nm). The higher RMS value under the dry condition was due to the existence of big craters caused by the aggregation of the zwitterionic phosphorylcholine groups in the poly(MPC)-grafted layer due to their strong intermolecular interactions. The decreased roughness of 10–0.25 in water was due to the reduced craters by the swelling of the poly(MPC)-grafted layer. The RMS roughness of the unmodified PDMS surface was 0.98 nm under the dry and 2.08 nm in water. Little difference in the RMS roughness of the unmodified PDMS under dry and wet conditions was due to the hydrophobic characteristics of the PDMS.

3.3. Protein adsorption

Fig. 8 shows the amount of albumin, γ-globulin, fibrinogen, and lysozyme adsorption on the membranes from the PBS buffer with 10% in vivo concentrations. There were little differences in the amount of adsorptions among the poly(MPC)-grafted PDMS membranes, which strongly agrees with the results of the surface characterization. The average amount of albumin adsorption on the poly(MPC)-grafted PDMS surfaces was 0.20 μg/cm^2, which was about a 70% reduction in the unmodified PDMS.

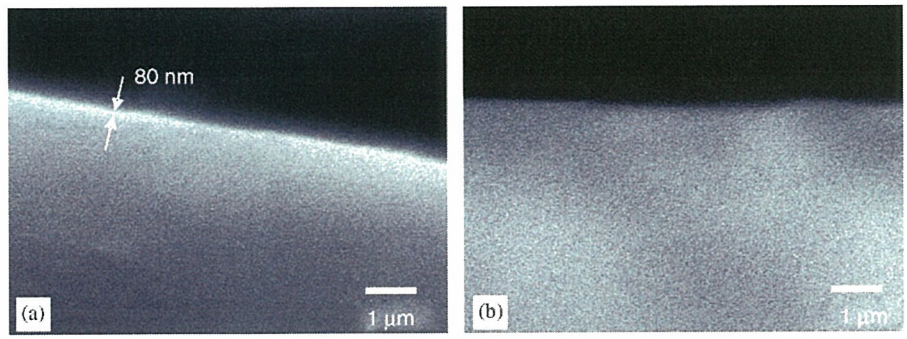

Fig. 6. SEM images of cross-sections of (a) surface modified PDMS and (b) unmodified PDMS membranes. The edge between the PDMS membranes in the picture of (a) and the air is evidenced by the poly(MPC) graft layer.

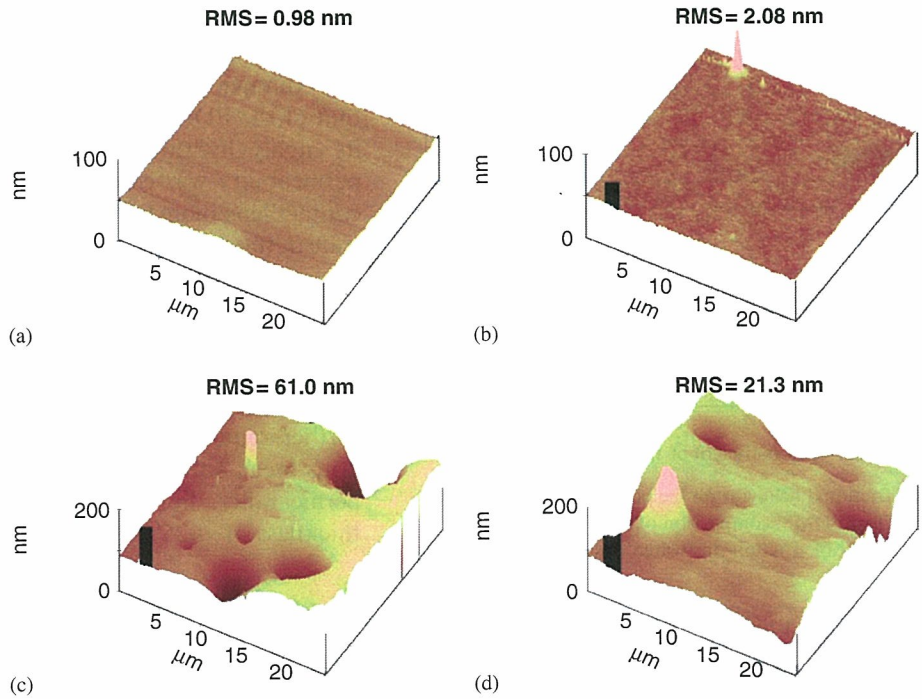

Fig. 7. AFM morphological images and root mean square roughness (RMS) values at 25 μm × 25 μm: unmodified PDMS surface under dry condition (a); unmodified PDMS surface in water (b); poly(MPC)-grafted PDMS (10–0.25) under dry condition (c); poly(MPC)-grafted PDMS (10–0.25) in water (d).

These results also agree with a previous report on the poly(MPC)-grafted surface [39]. As for γ-globulin, fibrinogen, and lysozyme, the adsorption amounts on the poly(MPC)-grafted PDMS membranes were 0.27, 0.28, and 0.15 μg/cm^2, which were, respectively, 50%, 75%, and 70% reductions compared with the unmodified PDMS. The mechanism of protein adsorption resistivity on the poly(MPC)-grafted surface is thought to be based on the interactions between water and the phosphorylcholine groups. The large amount of free water around the phosphorylcholine group is thought to repel proteins and even prevent conformational changes in the adsorbed proteins [29,40,41] The reduction in protein adsorption is also thought to be due to the presence of a thick hydrated layer around the phosphorylcholine group [26,42,43]. The determining factors for the protein adsorption behavior of the end-tethered polymer chains have been identified as the graft density, chain length, and chain conformation on the surface. Due to the bulkiness of the phosphorylcholine group in the side chain, the poly(MPC)-grated surfaces with a chain length greater than 50 monomer units are considered to be in the brush conformation even at a lower graft density (0.06 chains/nm^2) [32]. However, it is difficult to discuss the effect of the graft density of poly(MPC) due to the higher molecular weight distributions and the crosslinking between the graft chains prepared in this study.

3.4. Friction property

Fig. 9 shows the comparative frictional behavior on the poly(MPC)-grafted PDMS (10–0.25) and unmodified

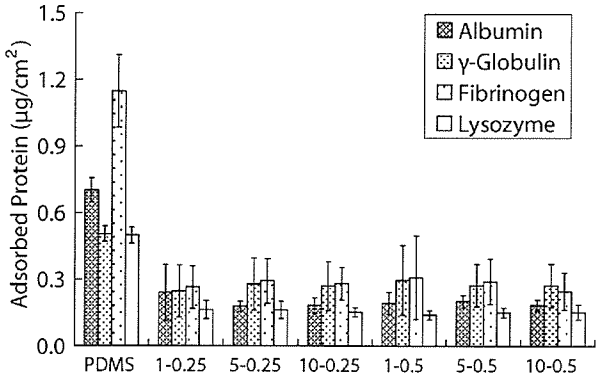

Fig. 8. Amount of single protein adsorption on the poly(MPC)-grafted PDMS surfaces with varying feed concentrations of initiator and monomer during polymerization.

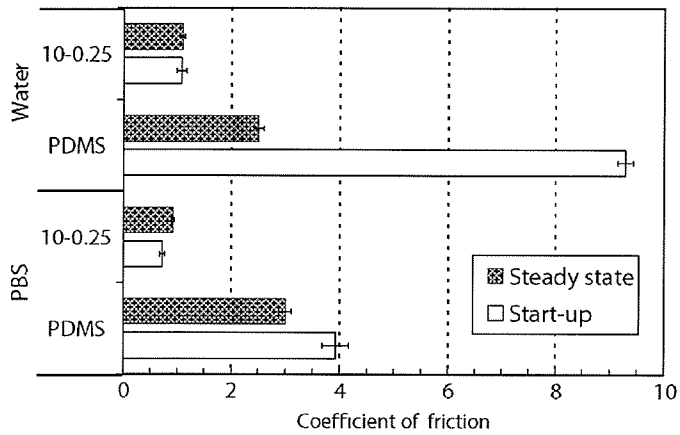

Fig. 9. Comparative frictional behavior on the poly(MPC)-grafted PDMS (10–0.25) and unmodified PDMS: comparison of start-up and steady state values of the coefficient of friction in water and in PBS at room temperature.

PDMS at start-up (static) and in the steady state (kinetic) condition in the presence of water and PBS. Generally, PDMS is known to possess a good adhesive property, and its adhesiveness is controlled by the cross-linker concentrations [44]. However, this characteristic was significantly altered by the poly(MPC) grafting. The static and kinetic friction coefficients on 10–0.25 in water were 1.071 and 1.091, respectively. These coefficients were 90% and 55% lower than those of the unmodified PDMS. The static and kinetic friction coefficients on 10–0.25 in PBS were 0.712 and 0.916, respectively. These coefficients were, respectively, 80% and 70% lower than those of the unmodified PDMS. The lowered frictional coefficients on the poly(MPC)-grafted PDMS was considered to be the presence of a hydration layer on the surface due to the water molecules tightly correlated to the phosphorylcholine groups in the poly(MPC). A computational simulation revealed the rapid adsorption and polarization of water molecules onto the phosphorylcholine group [40]. This hydrated poly(MPC) layer seem to serve as a lubricant. The kinetic friction coefficient on 10–0.25 in PBS was 15% lower than that in water although the reason is not clear.

3.5. Oxygen permeability

Oxygen permeability is an important factor for biomaterial applications, such as ophthalmologic biomaterials and an artificial lung so that the effect of the poly(MPC) grafting on the PDMS for oxygen permeability was checked by directly measuring the sample. Fig. 10 shows the dependence of the reciprocal of the electric current $I(t\rightarrow\infty)$ on the number n of moistened filter papers above each specimen with a given thickness. In Fig. 10, each slope was applied to have the same value due to the theory of transport phenomenon as determined by the least mean square method for all plots. The Dk_{membrane} of the poly(MPC)-grafted PDMS and unmodified PDMS calculated from Eqs. (5) and (6) were 334 and 335 barrers, respectively. The poly(MPC)-grafted PDMS maintained over 99% of the oxygen permeability due to its considerably thinner graft layer thickness (~100 nm) compared to that of the PDMS membrane (ca. 0.5 mm) and also due to its highly hydrated poly(MPC) graft layer. The oxygen permeability was extensively discussed in the field of soft contact lens biomaterials. It was suggested that the oxygen transmittance, Dk/L (Dk/t), for continuous wear soft contact lens should be 87–125 barrer/mm for a human cornea, which is equivalent to a no-lens situation [45–47] Considering the commercial soft contact lens thickness of $\leqslant 100\,\mu m$, this oxygen transmission requirement is easily obtained for the poly(MPC)-grafted PDMS. However, further requirements should be overcome for the continuous wear soft contact lens application, e.g., electrolyte permeability, lipid spoilation and controlled graft layer thickness of $\leqslant 25$ nm [8].

3.6. Tensile strength

The UV-induced free radical graft polymerization methods may pose a problem concerning the bulk mechanical property for the silicone elastomer. UV

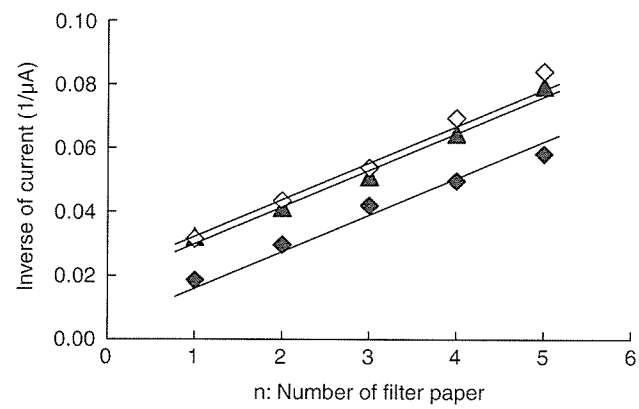

Fig. 10. Dependence of the reciprocal of electric current $I(t\rightarrow\infty)$ on the number n of moistened filter paper layers above poly(MPC)-grafted PDMS membrane (10–0.25; ◇), PDMS membrane (△) and the same plot for the results with only moistened filter paper layers in the experimental set-up (◆).

Table 2
Tensile test of the poly(MPC)-grafted PDMS membrane with different monomer and initiator conditions in the polymerization

Sample	Ultimate stress (MPa)	Ultimate strain (%)	Elastic modulus[a] (MPa)
PDMS	4.76±0.58	163±19	1.21±0.12
PDMS UV 5 h[b]	4.73±0.27	162±2	1.21±0.03
1–0.5	4.40±0.33	133±8	1.07±0.05
5–0.5	4.30±0.51	145±14	1.04±0.03
10–0.5	4.49±0.70	147±11	1.10±0.05

[a]Determined by the range of initial 1% of the strain.
[b]UV-irradiated PDMS for 5 h without initiator under dry condition.

irradiation may affect the elasticity of the material due to the formation of crosslinks by the combination of radials in the bulk phase of the PDMS. Tensile tests were performed on the poly(MPC)-grafted PDMS membranes to determine the effect for the bulk phase of PDMS. The UV-irradiated PDMS without initiator adsorption was also checked in order to discuss the affect of radicals on the bulk behavior. Table 2 shows the result of the ultimate stress, ultimate strain and elastic modulus for the poly(MPC)-grafted PDMS. Both the ultimate stress and strain of the poly(MPC)-grafted PDMS were lower than those of the unmodified PDMS by about 10%. Small decreases in the elastic modulus were also observed within the initial 1% strain regions for the poly(MPC)-grafted PDMS. No decrease in the mechanical property of the PDMS was seen after the UV irradiation of 5 h. Although the deterioration of the PDMS bulk phases occurred due to radicals, they seem to be too limited to affect the PDMS practical uses.

4. Conclusion

We reported the preparation of a biomimetic poly(MPC)-grafted PDMS in order to enhance its surface hydrophilicity, anti-biofouling property, and biocompatibility. A convenient polymerization was conducted using the UV-induced free radical "grafting-from" method based on the physically adsorbed benzophenone on the PDMS. The graft layer thickness was controlled by the UV irradiation time. The surface properties were more significantly influenced by the physically adsorbed initiator amount than the monomer concentration. Reductions of the adsorbed single proteins on the poly(MPC)-grafted PDMS membranes were about 50–75%. Comparative frictional experiments revealed the reduced friction coefficients on the poly(MPC)-grafted PDMS under wet conditions. The presence of a highly hydrated thick water layer around the poly(MPC) graft chains is seem to reduce both the protein adsorption and surface friction. The poly(MPC)-grafted PDMS maintained the high oxygen permeability and tensile property of the PDMS. The poly(MPC)-grafted PDMS is attractive for medical elastomers and microfluidic materials.

Acknowledgments

We are indebted to Dr. T. Hanawa, Dr. Y. Iwasaki and Ms. R. Iwata at Tokyo Medical and Dental University for the ellipsometric experiments. The author (T.G) thank the partial support of a Grant for 21st Century COE Program for "Human-Friendly Materials based on Chemistry" from MEXT of Japan.

References

[1] Motomura T, Maeda T, Kawahito S, Matsui T, Ichikawa S, Ishitoya H, et al. Development of silicone rubber hollow fiber membrane oxygenator for ECMO. Artif Organs 2003;27:1050–3.
[2] Joyce TJ, Unsworth A. The wear of artificial finger joints using different lubricants in a new finger wear simulator. Wear 2001; 250:199–205.
[3] Eteshola E, Leckband D. Development and characterization of an ELISA assay in PDMS microfluidic channels. Sensor Actuator B—Chem 2001;72:129–33.
[4] Zwischenberger JB, Anderson CM, Cook KE, Lick SD, Mockros LF, Bartlett RH. Development of an implantable artificial lung: challenges and progress. ASAIO J 2001;47:316–20.
[5] Huck TSW, Bowden N, Onck P, Pardoen T, Hutchinson JW, Whitesides GM. Ordering of spontaneously formed buckles on planar surfaces. Langmuir 2000;16:3497–501.
[6] Ouyang M, Yuan C, Muisener RJ, Boulares A, Koberstein JT. Conversion of some siloxane polymers to silicon oxide by UV/ozone photochemical processes. Chem Mater 2000;12:1591–6.
[7] Lai JY, Lin YY, Denq YL, Chen JK. Surface modification of silicone rubber by gas plasma treatment. J Adhes Sci Technol 1996;10:231–42.
[8] Tighe B. Silicone hydrogels: structure, properties and behaviour. In: Sweeney DF, editor. Silicone hydrogels. Continuous-wear contact lenses. 2nd ed. London: W1T; 2004. p. 1–27.
[9] Chaudhury MK, Whitesides GM. Direct measurement of interfacial interactions between semispherical lenses and flat sheets of poly-(dimethylsiloxane) and their chemical derivatives. Langmuir 1991;7: 1013–25.
[10] Hillborg H, Tomczak N, Olah A, Schoonherr H, Vancso G. Nanoscale hydrophobic recovery: a chemical force microscopy study of UV/Ozone-treated cross-linked poly(dimethylsiloxane). Langmuir 2004;20:785–94.
[11] Olah A, Hillborg H, Vancso GJ. Hydrophobic recovery of UV/ozone treated poly(dimethylsiloxane): adhesion studies by contact mechanics and mechanism of surface modification. Appl Surf Sci 2005;239:410–23.
[12] Xia Y, Whitesides GM. Soft lithography. Angew Chem Int Ed 1998;37:550–75.
[13] Ishihara K, Sibarani J, Takai M. Protein adsorption resistance by biocompatible phospholipid polymers as a surface modification on PDMS. Proc μ-TAS 2005;1:253–5.
[14] Zhao B, Brittain WJ. Polymer brushes: surface-immobilized macromolecules. Prog Polym Sci 2000;25:677–710.
[15] Zajac R, Chakrabarti A. Irreversible polymer adsorption from semidilute and moderately dense solutions. Phys Rev E 1995;52: 6536–49.
[16] Ito Y, Ochiai Y, Park YS, Imanishi Y. pH-sensitive gating by conformational change of a polypeptide brush grafted onto a porous polymer membrane. J Am Chem Soc 1997;119:1619–23.
[17] Prucker O, Ruhe J. Synthesis of poly(styrene) monolayers attached to high surface area silica gels through self-assembled monolayers of azo initiators. Macromolecules 1998;31:592–601.

[18] Husseman M, Malmstrom EE, McNamara M, Mate M, Mecerreyes D, Benoit DG. Controlled synthesis of polymer brushes by "living" free radical polymerization techniques. Macromolecules 1999;32: 1424–31.
[19] Pyun J, Kowalewski T, Matyjaszewski K. Synthesis of polymer brushes using atom transfer radical polymerization. Macromol Rapid Commun 2003;24:1043–59.
[20] Miller PJ, Matyjaszewski K. Atom transfer radical polymerization of (meth)acrylates from poly(dimethylsiloxane) macroinitiator. Macromolecules 1999;32:8760–7.
[21] Ishihara K, Aragaki R, Ueda T, Watanabe A, Nakabayashi N. Reduced thrombogenicity of polymers having phospholipid polar groups. J Biomed Mater Res 1990;24:1069–77.
[22] Ishihara K, Ziats NP, Tierney BP, Nakabayashi N, Anderson JM. Protein adsorption from human plasma is reduced on phospholipid polymers. J Biomed Mater Res 1991;25:1397–407.
[23] Ishihara K, Oshida H, Endo Y, Ueda T, Watanabe A, Nakabayashi N. Hemocompatibility of human whole blood on polymers with a phospholipid polar group and its mechanism. J Biomed Mater Res 1992;26:1543–52.
[24] Sugiyama K, Ohga K, Aoki H. Emulsion copolymerization of 2-(acryloyloxy)ethylphosphorylcholine with vinyl monomers and protein adsorption at resultant copolymer microspheres. Macromol Chem Phys 1995;196:1907–16.
[25] Oishi T, Uchiyama H, Onimura K, Tsutsumi H. Synthesis and properties of poly(methacrylate) bearing a phosphorylcholine analogous group. Polym J 1998;30:17–22.
[26] Ruiz L, Hilborn JG, Leonard D, Mathieu HJ. Synthesis, structure and surface dynamics of phosphorylcholine functional biomimicking polymers. Biomaterials 1998;19:987–98.
[27] Wang Y, Su TJ, Green R, Tang Y, Styrkas D, Danks TN, et al. Covalent coupling of an phospholipid monolayer on the surface of ceramic materials. Chem Commun 2000;0:587–8.
[28] Ishihara K, Ueda T, Nakabayashi N. Preparation of phospholipid polymers and their properties as polymer hydrogel membrane. Polym J 1990;22:355–60.
[29] Ishihara K, Nomura H, Mihara T, Kurita K, Iwasaki Y, Nakabayashi N. Why do phospholipid polymers reduce protein adsorption? J Biomed Mater Res 1998;39:323–30.
[30] Kitano H, Imai M, Mori T, Gemmei-Ide M, Yokoyama Y, Ishihara K. Structure of water in the vicinity of phospholipid analog copolymers as studied by vibrational spectroscopy. Langmuir 2003; 19:10260–6.
[31] Feng W, Zhu S, Ishihara K, Brash JL. Protein resistant surfaces: comparison of acrylate graft polymers bearing oligo-ethylene oxide and phosphorylcholine side chains. Biointerphases 2006;1: 50–60.
[32] Ishihara K, Iwasaki Y, Ebihara S, Shindo Y, Nakabayashi N. Photoinduced graft polymerization of 2-methacryloyloxyethyl phosphorylcholine on polyethylene membrane surface for obtaining blood cell adhesion resistance. Colloid Surf B—Biointerfaces 2000;18: 325–35.
[33] Moro T, Takatori Y, Ishihara K, Konno T, Takigawa Y, Matushita T, et al. Surface grafting of artificial joints with a biocompatible polymer for preventing periprosthetic osteolysis. Nature Mater 2004;3:829–36.
[34] Inoue Y, Watanabe J, Ishihara K. Dynamic motion of phosphorylcholine groups at the surface of poly(2-methacryloyloxyethyl phosphorylcholine-random-2,2,2-trifluoroethyl methacrylate). J Colloid Interface Sci 2004;274:465–71.
[35] Compañ V, Villar MA, Vallés E, Riande E. Permeability and diffusional studies on silicone polymer networks with controlled dangling chains. Polymer 1996;37:101–7.
[36] Compañ V. A potentiostatic study of oxygen transport through poly(2-ethoxyethyl methacrylate-*co*-2,3-dihydroxypropylmethacrylate) hydrogel membranes. Biomaterials 2005;26:3783–91.
[37] Compañ V, Guzmán J, Riande E. A potentiostatic study of oxygen transmissibility and permeability through hydrogel membranes. Biomaterials 1998;19:2139–45.
[38] Moore WM, Hammond GS, Foss RP. Mechanisms of photoreactions in solutions. 1. reduction of benzophenone by benzhydrol. J Am Chem Soc 1961;83:2789–94.
[39] Iwasaki Y, Saito N. Immobilization of phosphorylcholine polymers to Ti-supported vinyldimethylsilyl monolayers and reduction of albumin adsorption. Colloids Surf B—Biointerface 2003;32:77–84.
[40] Sheng Q, Schulten K, Pidgeon C. Molecular dynamics simulation of immobilized artificial membranes. J Phys Chem 1995;99:11018–27.
[41] Goda T, Watanabe J, Takai M, Ishihara K. Water structure and improved mechanical properties of phospholipid polymer hydrogel with phosphorylcholine centered intermolecular cross-linker. Polymer 2006;47:1390–6.
[42] Kitano H, Kawasaki A, Kawasaki H, Morokoshi S. Resistance of zwitterionic telomers accumulated on metal surfaces against nonspecific adsorption of proteins. J Colloid Interface Sci 2005;282: 340–8.
[43] Feng W, Zhu S, Ishihara K, Brash JL. Adsorption of fibrinogen and lysozyme on silicon grafted with poly(2-methacryloyloxyethyl phosphorylcholine) via surface-initiated atom transfer radical polymerization. Langmuir 2005;21:5980–7.
[44] Carrillo F, Gupta S, Balooch M, Marshall SJ, Marshall GW, Pruitt L, et al. Nanoindentation of polydimethylsiloxane elastomers: effect of crosslinking, work of adhesion, and fluid environment on elastic modulus. J Mater Res 2005;20:2820–30.
[45] Harvitt D, Bonanno J. Re-evaluation of the oxygen diffusion model for predicting minimum contact lens Dk/t values needed to avoid corneal anoxia. Optom Vis Sci 1999;76:712–9.
[46] Grobe GL, Kunzler JF, Seelye D, Salamone JC. Silicone hydrogels for contact lens application. Polym Mater Sci Eng 1999;80:108–9.
[47] Nicolson PC, Vogt J. Soft contact lens polymers: an evolution. Biomaterials 2001;22:3273–83.

Available online at www.sciencedirect.com
SCIENCE DIRECT
polymer
Polymer 47 (2006) 1390–1396
www.elsevier.com/locate/polymer

Water structure and improved mechanical properties of phospholipid polymer hydrogel with phosphorylcholine centered intermolecular cross-linker

Tatsuro Goda, Junji Watanabe, Madoka Takai, Kazuhiko Ishihara *

Department of Materials Engineering, School of Engineering, The University of Tokyo, 7-3-1, Hongo, Bunkyo-ku, Tokyo 113-8656, Japan

Received 12 May 2005; received in revised form 1 November 2005; accepted 11 December 2005
Available online 18 January 2006

Abstract

We investigated the water structure and the mechanical properties of 2-methacryloyloxyethyl phosphorylcholine (MPC) polymer hydrogels cross-linked with a novel hydrophilic 2-(methacryloyloxy)ethyl-[*N*-(2-methacryloyloxy)ethyl]phosphorylcholine (MMPC) for soft contact lenses (SCL) applications and commercial methacrylic cross-linkers were in addition used for comparison with MMPC. Water structure in hydrogels, which influences the protein adsorption by dehydration was determined by differential scanning calorimetry. MMPC increased the freezing water content of the MPC polymer hydrogel compared with hydrophilic *N*,*N*′-methylenebisacrylamide (BIS) at the same water content. MMPC also improved fracture strength of the MPC polymer hydrogel to 120 kPa in tensile, which was considerably higher than that hydrogel cross-linked with BIS. It is suggested that MMPC shows higher cross-linking reactivity with MPC than BIS. We concluded that the MMPC increase both the free water content and the tensile properties. The MPC polymer hydrogel cross-linked with MMPC can be a useful SCL biomaterial.
© 2005 Elsevier Ltd. All rights reserved.

Keywords: Hydrogel; Hydrophilic cross-linker; Phospholipid polymer

1. Introduction

Chemically cross-linked polymer hydrogels that in addition have a high water percentage possess several unique characteristics such as elasticity, softness, transparency and permeability [1–4]. As a result, such hydrogels are widely used for low elastic biomedical applications and have been used in a broad range of product [5,6]. Specifically, 2-hydroxyethyl methacrylate (HEMA) is a frequently used soft contact lenses (SCL) material [5]. We have intensively studied biomaterials based on original bioinspired polymer containing 2-methacryloyloxyethyl phosphorylcholine (MPC) (Fig. 1(a)), due to their excellent biocompatibility, blood-compatibility and anti-fouling properties [7–14]. The unique characteristics of MPC originate from the zwitterionic phosphorylcholine headgroup found in the biological membrane. Recent reports have described some fundamental aspects on the synthesis and characterization on MPC based hydrogels cross-linked with commercially available methacrylic cross-linker, such as triethylene glycol dimethacrylate (TEGDMA) and ethylene glycol dimethacrylate (EGDMA) [15,16].

In this report, we have focused on the physical properties of MPC polymer hydrogels for the SCL application. In general, the high water content of hydrogels cause mechanical weaknesses and reduced biocompatibility due to dehydration of the lens [17]. To overcome this, the equilibrium water content (EWC) of the MPC polymer hydrogel need to be adjusted to around 80%, which is equal to that of cornea. A typical approach to adjust the EWC is to regulate the cross-link density in the hydrogel network. Usually, MPC polymer hydrogels cross-linked with TEGDMA and EGDMA provide an EWC that is too high (over 90%), since the hydrophobicity of their cross-linker limit their solubility in aqueous media to about 1 mol% [15,16]. To control the EWC and cross-link density of MPC polymer hydrogel, hydrophilic cross-linkers are needed. In addition, previous papers reported the water structure on the MPC polymer-coated surface on various polymers and protein adsorption onto a polymer surface is strongly related to the 'free water' contents around polymer chains [8,13]. Thus the water structure in hydrogel networks is important because anti-fouling properties are required for SCL material.

To satisfy these requirements, we used a new type of MPC based intermolecular cross-linker having

* Corresponding author. Tel.: +81 3 5841 7124; fax: +81 3 5841 8647.
E-mail address: ishihara@mpc.t.u-tokyo.ac.jp (K. Ishihara).

0032-3861/$ - see front matter © 2005 Elsevier Ltd. All rights reserved.
doi:10.1016/j.polymer.2005.12.043

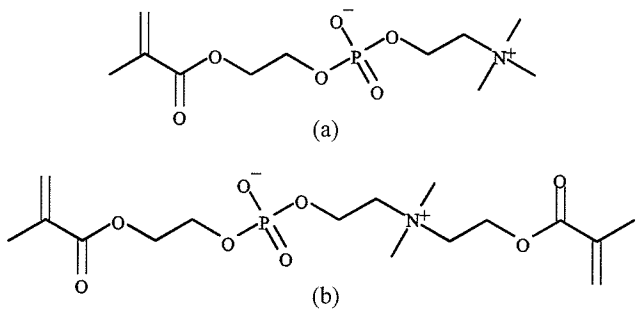

Fig. 1. Chemical structure of phospholipid monomers, (a) MPC and (b) MMPC.

a phosphorylcholine-like group in the center of the molecule previously reported by us: 2-(methacryloyloxy)ethyl-[*N*-(2-methacryloyloxy)ethyl]phosphorylcholine (MMPC) (Fig. 1(b)) [18]. This is a hydrophilic MPC analogue developed to have affinity both to water and to the methacrylic cross-linking units. MMPC was expected not only to adjust the EWC, cross-link density and to enhance the mechanical strength but also to increase the free water content of the MPC polymer hydrogel. A hydrophilic cross-linker; *N*,*N*′-methylenebisacrylamide (BIS), is commercially available and often used as a cross-linking reagent for acryl amide and *N*-isopropyl acrylamide in aqueous media [19], was used as a reference. In this paper, we discuss the differences between MMPC and BIS for adjusting the EWC, cross-link density, water structure, and the mechanical properties of MPC polymer hydrogels. In addition, the transparency of the MPC polymer hydrogel in the visible light wavelength was evaluated for SCL applications.

2. Experimental

2.1. Materials

MPC [7], MMPC [18] were prepared by previous methods. TEGDMA, EGDMA (Tokyo Kasei, Tokyo, Japan) and BIS (Kanto Chemical, Tokyo, Japan) were used without further purification. Ammonium peroxodisulfate (APS, Kanto Chemical) and *N*,*N*,*N*′,*N*′-tetramethylethylenediamine (TMEDA, Kanto Chemical) were extra-pure grade reagents. All other solvents were extra-pure reagent grade and used without further purification. Phosphate buffer saline (PBS) stock solution (#14200-075, Invitrogen Co., Tokyo, Japan) was diluted and used with tenth.

2.2. Preparation of MPC polymer hydrogel

The MPC aqueous solution (2.5 mol/L), a cross-linker, and 1.3 mol% of APS aqueous solution (0.22 mol/L) as an initiator were placed on a Petri dish. MMPC and BIS were used from 1.0 to 5.0 mol% for monomer concentration. The contents to reach higher concentration of TEGDMA and EGDMA were limited up to 1.0 mol% of monomer because of their hydrophobicity. The solution in the Petri dish was stirred for 30 min to be fully mixed. Then, as a catalyst, TMEDA was added and stirring was continued for another 30 s. The solution was placed in a reaction spacer containing a pair of plastic plates with 0.1–1.0 mm thickness. The obtained MPC polymer hydrogel was immersed in excess distilled water for 2 days for swelling and purification. The water was changed several times. The purified and equilibrated MPC polymer hydrogel was cut into desired shapes. We abbreviated the MPC polymer hydrogels by concentration of the initial alphabet of cross-linker and concentrations in feed (Table 1).

Table 1
Preparation condition of MPC polymer hydrogel

Code	Cross-linker	Concentration in feed (mol%)	MPC in feed (mol/L)
M1	MMPC	1.0	2.5
B1	BIS	1.0	2.5
E1	EGDMA	1.0	2.5
T1	TEGDMA	1.0	2.5
M3	MMPC	3.0	2.5
B3	BIS	3.0	2.5

2.3. Characterization of MPC polymer hydrogel

The transparency of MPC polymer hydrogel was examined by using UV/vis spectrophotometer (V-560, JASCO, Tokyo, Japan). The measurements were performed from 230 to 700 nm wavelength with 1.0 mm thickness of MPC polymer hydrogels at room temperature.

The EWC of MPC polymer hydrogel was determined by gravimetrical method. Dried hydrogels were obtained by lyophilization. The equation of the EWC is as follows;

$$\mathrm{EWC}\% = \left(1 - \frac{W_\mathrm{d}}{W_\mathrm{s}}\right) \times 100$$

Here, W_d is the weight of dried hydrogel and W_s is the weight of swollen hydrogel. The numbers of specimens were five. We also evaluated the EWC changes of MPC polymer hydrogel and commercial SCL in PBS (pH=7.1, 0.01 mol/L). The method is the same as pure water system.

Differential scanning calorimetry (DSC) equipment (DSC 6100, Seiko Instruments, Chiba, Japan) was used to measure thermal properties of polymer hydrogel, such as the glass transition temperature (T_g). The weight of 3–5 mg of a lyophilized hydrogel was sealed in the aluminum (Al) pan and the heating measurements were performed from −100 to 250 °C at a rate of 10 °C/min. The Al pans were sonicated in acetone before use. The amount of the phase transition of water in the hydrogel was calculated by enthalpy of fusion around 0 °C on heating process. After the surplus water was removed by filter paper, a piece of about 5–10 mg weight was cut off and weighed accurately. Then, specimen was sealed in Al pan not to dehydrate. The DSC curves were monitored both cooling and heating run from −50 to 50 °C at a rate of 5 °C/min.

The fracture stress and strain (S–S) of MPC polymer hydrogels were examined using a tensile test machine (STA-1150, ORIENTEC, Tokyo, Japan). The samples were cut into a dumbbell shape (12.5 mm×2.5 mm×1.0 mm) and

strained with 10 mm/min cross-head speed. Each hydrogel was examined five times. Compression measurements were performed on the hydrogels using a compressive tester (TMA/SS6000, Seiko Instruments, Japan). The cylindrical hydrogel samples of 10 mm in diameter and 1.5 mm thickness were set on the lower stage and compressed by the probe (2.6 mm in diameter) using a step mode at 25 °C. Measurements were performed five times for each sample and the result was statistically calculated. All the hydrogels were sprayed with water not to dehydrate on their surfaces in the mechanical experiments.

3. Results and discussion

3.1. Transparency

Fig. 2 shows the light transmittance of M1 and E1 for the thickness of 0.1 mm calculated by the Bouguer's conversion and that of ACUVUE® (Johnson and Johnson, USA) which is a commercially available sample in the visible light wave range (230–700 nm). MPC polymer hydrogels with any cross-linker exhibited the high transparency in the wide range of the wavelength. The transmittance for ACUVUE® suddenly decreased below 350 nm because of the UV protection treatment. Usually, benzotriazole or benzophenone is incorporated for UV absorbing. Therefore, MPC polymer hydrogel may also have UV protecting ability by incorporation with them. These results indicate that MPC polymer hydrogels are useful SCL biomaterials in terms of light transmittance in the range of visible light wavelengths.

3.2. EWC in water and PBS

Fig. 3 shows the relations between the EWC of MPC polymer hydrogel and the in feed cross-linker concentration. The EWC of the MPC polymer hydrogels decreased with an increased cross-linker concentration in feed and especially

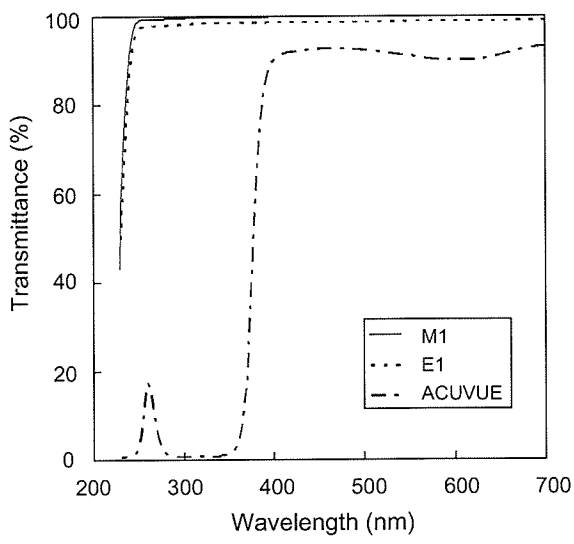

Fig. 2. Transparency of MPC polymer hydrogels and commercial SCL (ACUVUE®).

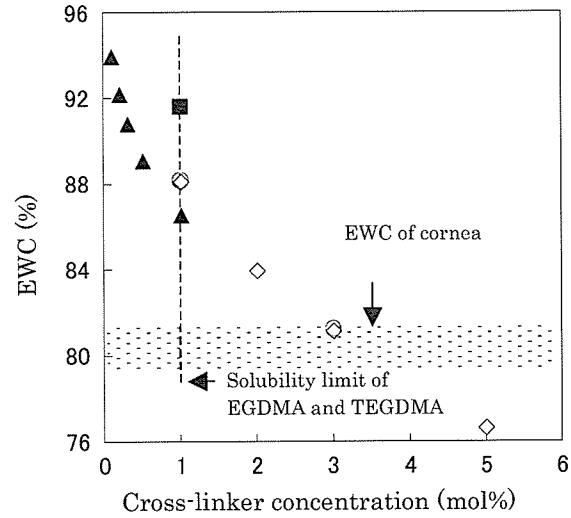

Fig. 3. EWC change of MPC polymer hydrogel by alteration of cross-linker concentration in feed, MMPC (◇), BIS (○), EGDMA (▲), TEGDMA (■).

MMPC enabled to adjust the EWC to that of cornea (82%) [20] at 3 mol% (M3). Conventional methacrylic cross-linkers, TEGDMA and EGDMA were not able to adjust the EWC to around 82% for SCL materials because their hydrophobicity prevents hydrogel preparation over 1 mol% in feed. BIS also suppressed the EWC of the MPC polymer hydrogels to around 82%. There were little differences between MMPC and BIS with regards to the EWC.

No EWC change of MPC polymer hydrogels between those in water and PBS was observed. This was because the MPC polymer chain is zwitterionic and thus electroneutral; which was based on the salt formation in the each MPC unit. This result denoted that the MPC polymer hydrogel has the volume stability for ionic strength, which is important for optical system. However, the EWC of ACUVUE® decreased from 69% to 58% by soaking in water to PBS solution. Because ACUVUE® is the copolymer of HEMA and methacrylic acid (MA), the carboxyl group of MA is affected by ions of salt solution and water molecules in the hydrogel were pulled away to counterbalance by the osmotic pressure.

3.3. Water structure in MPC polymer hydrogels

Generally, the water structure in the polymer hydrogel can be distinguished into 'free water', 'freezing bound water', and 'non-freezing bound water' [21,22]. Free water does not take part in hydrogen bonding with polymer molecules. It has a similar transition temperature, enthalpy and DSC curves as pure water. Freezing bound water interacts weakly with polymer molecules. Non-freezing bound water is complex with the polymer chain through hydrogen bonds. We categorized the water structures in the hydrogel into three types. The total content of freezing water ($W_{freezing}$) was calculated by DSC, from the area under the endothermic curve for water-swollen hydrogels to melting endothermic heat of fusion for pure water. The calibration of the instrument with pure water yielded the enthalpy of fusion of water as $\Delta H_w = 333.3$ J/g, and this value

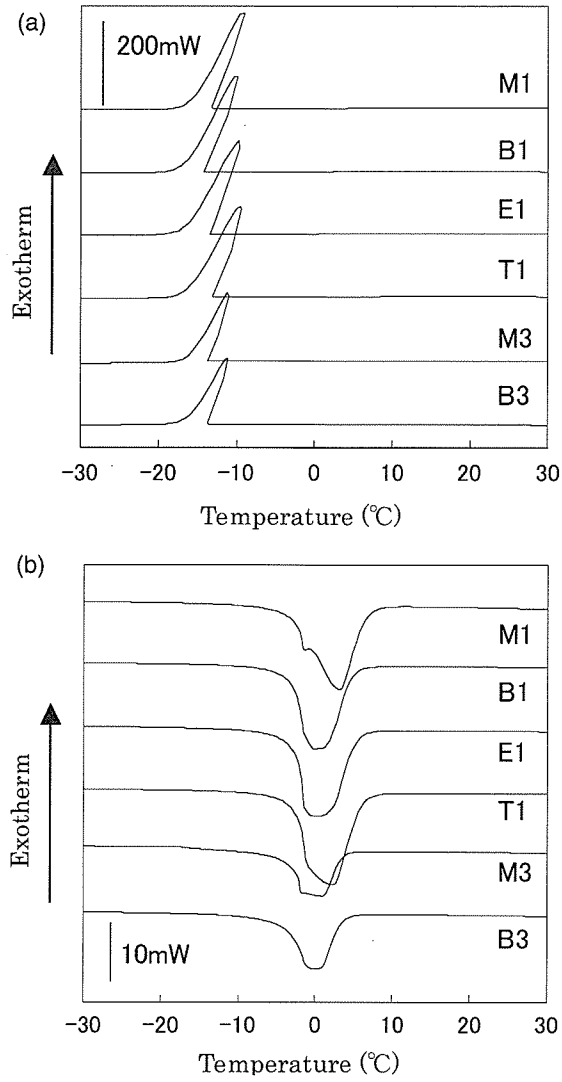

Fig. 4. DSC thermograms of MPC polymer hydrogels. Exothermic curves on cooling (a) and endothermic curves on heating (b). Free water in the hydrogel was supercooled (a). The enthalpy of fusion of freezing water was observed at 0 °C and broad shoulder peak of freezing bound water was detected.

was used to calculate the weights of water in the various states. Fig. 4 displays the thermograms obtained during the cooling run for MPC polymer hydrogel from 30 to −30 °C (a) and the heating run from −30 to 30 °C (b). The recrystallization transitions were shifted to lower temperature by about 16 degrees, and the integrated enthalpies of crystallization gave lower values than those of the melting transitions. The peak shape and the maximum peak temperature were dependent on the cooling and heating rates [23]. Normally, the sharp and clear peak originated from freezing bound water is observed around −10 °C at heating process for some HEMA based hydrogels and this freezing bound water is often referred to as 'intermediate water' [24]. In the MPC polymer hydrogels, the small sharp peaks and the broad peaks of freezing bound water were detected. The hydrogels showed the broad shoulder peaks from −30 to −5 °C originated from the freezing bound water. No further endothermic peak was observed to −100 °C in the cooling run. The shoulder peak area of freezing bound water was

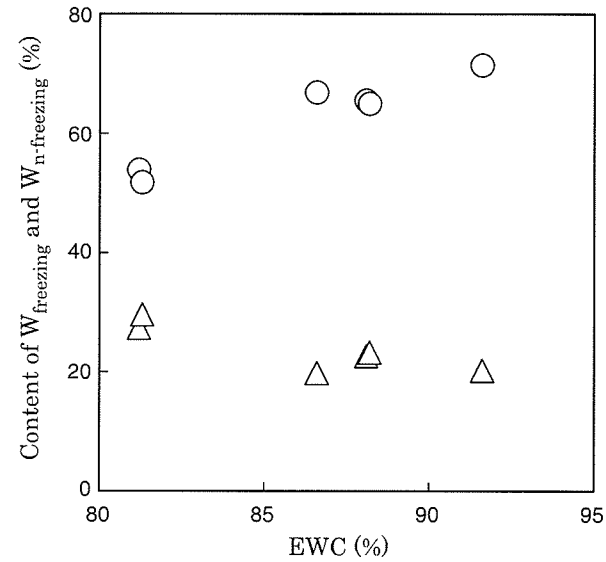

Fig. 5. Relationships between free water contents ($W_{freezing}$, ○) and bound water contents ($W_{n\text{-}freezing}$, △) for EWC on MPC polymer hydrogels.

very low and lapped over free water. The total contents of free water (W_{free}) and freezing bound water ($W_{f\text{-}bound}$) were determined by direct integration of the endothermic peaks from about −30 to 10 °C (ΔH).

$$W_{freezing} = W_{free}(\%) + W_{f\text{-}bound}(\%) = \frac{\Delta H}{\Delta H_w} \times 100$$

We also determined the content of non-freezing bound water ($W_{n\text{-}freezing}$) indirectly by subtracting $W_{freezing}$ from the EWC.

$$W_{n\text{-}freezing}(\%) = EWC - W_{freezing}$$

In this equation, the quantities of freezing water and non-freezing bound water are calculated as weights relative to the total weight of swollen hydrogel and expressed finally as percentages [21]. The $W_{freezing}$ calculated by the endothermic peak on heating run for each hydrogel is summarized in Table 2 and the calculated mean values are presented. Their statistical errors were all within 4%. Small differences of the water structure in the MPC polymer hydrogels caused by the type of cross-linker were observed. The MPC polymer hydrogels cross-linked with MMPC showed higher percentage of $W_{freezing}$ and lower percentage of $W_{n\text{-}freezing}$ than that of cross-linked with BIS unless their EWC were almost the same. This tendency became clearer at 3 mol% than 1 mol%. This result indicated that MMPC has a weak interaction to water molecules compared

Table 2
Water structure in MPC polymer hydrogels and ACUVUE®

Code	EWC (%)	$W_{freezing}$ (%)	$W_{n\text{-}freezing}$ (%)	$W_{freezing}/W_{n\text{-}freezing}$
M1	88.1	65.5	22.6	2.9
B1	88.2	65.0	23.1	2.8
E1	86.6	66.8	19.8	3.4
T1	91.6	71.4	20.2	3.5
M3	81.2	53.9	27.3	2.0
B3	81.3	51.7	29.6	1.8
ACUVUE®	69.0	45.6	23.4	2.0

with BIS. In other words, the mobility of water molecules around MMPC keeps the state of bulk water rather than that of BIS. Fig. 5 shows the relations between the EWC and the content of $W_{freezing}$ and $W_{n\text{-}freezing}$ of MPC polymer hydrogel. When decreasing the EWC from 90 to 80%, the content of $W_{n\text{-}freezing}$ increased about 10% while the content of $W_{freezing}$ decreased about 20%. These rapid changes on $W_{n\text{-}freezing}$ and $W_{freezing}$ were caused by the change in polymer density in the MPC polymer hydrogels.

3.4. Mechanical properties of MPC polymer hydrogel

Fig. 6 exhibits the tensile stress (σ) and strain (ε) relations at fracture points of MPC polymer hydrogels with various cross-linkers and in feed concentrations. All the hydrogels showed linear S–S relations, that is, elastic deformations. When increasing the MMPC or BIS content in the MPC polymer hydrogel, the fracture stress and elastic modulus (E_T) increased, while elongation at break point decreased. M3 and B3 had similar EWC and E_T, however, the fracture stress of M3 was 170% higher than that of the B3. This suggests that the tensile performances are more related to chain distribution and entanglement and less dependent on the water content. We suggest that these differences originate from the increased of cross-linker, that is, the methacrylic cross-linker MMPC has better reactivity for MPC than the acrylic cross-linker BIS. Fracture stress and strain were also dependent on the cross-linker type at a concentration of 1 mol%. The results indicate that the change of cross-linker has a pronounced effect on tensile properties and nano-structure of the hydrogels.

To examine the elasticity of the MPC polymer hydrogels, compression tests were performed. Fig. 7 shows the $S(\sigma)-S(1-\varepsilon)$ curves obtained for the MPC polymer hydrogel cross-linked with MMPC. As a reference, *S–S* relation for five-plied ACUVUE® was checked in the same way. Comparing the M3 and ACUVUE® curves, there is a difference in the compression

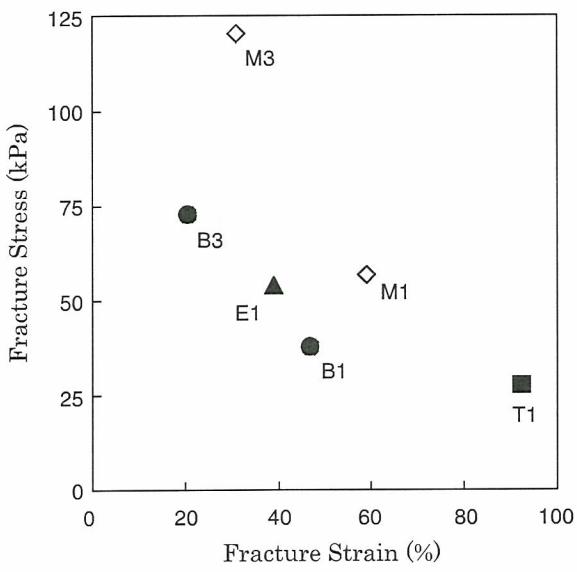

Fig. 6. Tensile tests representing the relationship between stress and strain of the MPC polymer hydrogels with various cross-linkers at fracture points.

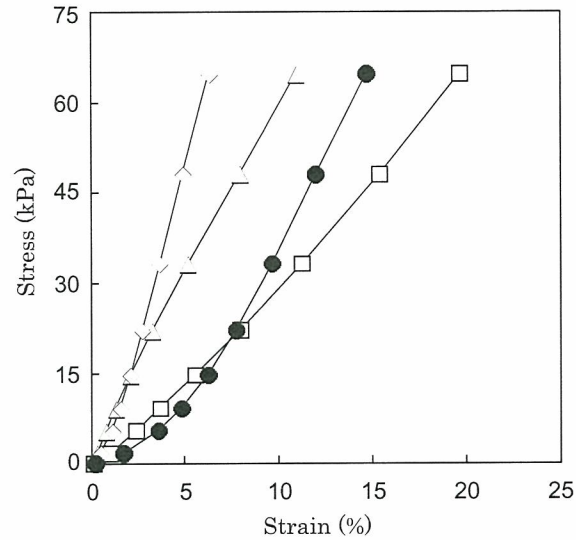

Fig. 7. Compression tests on M1 (□), M2 (△), and M3 (◇) compared with ACUVUE® (●).

strain at tensions below 15 kPa. Above 15 kPa the *S–S* curve for ACUVUE® became linear and there is no obvious difference between the modulus of the materials. M3 still keeps the same *S–S* relation as ACUVUE® in this range. When increasing the MMPC concentrations, the *S–S* curves became steep, due to the higher cross-link density in the polymer hydrogel.

3.5. Cross-link density and distance

According to the theory of rubber elasticity, the elastic modulus is related to the effective network chain concentration of the swollen hydrogel, v_e/V (cross-link density) by the following equation [25,26].

$$\frac{v_e}{V} = \frac{\sigma(\varphi_2/\varphi_0)^{2/3}}{RT|\alpha-\alpha^{-2}|}$$

where σ is in the unit of Pa, v_e/V is in mol/m^3, φ_2 is the volume fraction at swollen state, φ_0 is the swelling fraction (W_d/W_s), R is 8.314 J/mol K, T is the absolute temperature in K and α is the deformation ratio. The deformation ratio α is the ratio of elastically deformed length L to initial length L_0 of the hydrogel. Cross-link densities were calculated by the fracture point for tensile and by 5% strain point for compression [27], respectively. Further, the averaged cross-link distance (mesh size), ξ was estimated from the cross-link density using the following equation.

$$\xi = \left(\frac{N_A v_e}{V}\right)^{-1/3}$$

where N_A is the Avogadro's number. The cross-link densities, v_e/V, averaged mesh size, ξ, calculated by the tensile and compression results were listed on the Table 3. The EWC and the cross-link density of M1 was the same as B1 at tensile mode. This relation was valid between M3 and B3, too. These results prove that the same EWC represent the same cross-link

Table 3
Estimated cross-link densities and cross-link distances calculated from the Young's modulus

Code	φ_2	φ_0	Tensile		Compression	
			ν_e/V (mol/m^3)	ξ (nm)	ν_e/V (mol/m^3)	ξ (nm)
M1	0.09	0.12	16	4.7	33	3.7
B1	0.12	0.12	16	4.7	25	4.1
E1	0.12	0.13	23	4.1	49	3.2
T1	0.07	0.08	6	6.6	11	5.3
M3	0.16	0.19	60	3.0	87	2.7
B3	0.21	0.19	61	3.0	81	2.7

density. Table 3 also indicates that the EWC of MPC polymer hydrogel decrease when increasing the cross-link density. The supplemental observation from Table 3 is that the cross-link densities in compression mode were higher than those of in tensile mode for each hydrogel. However, the reason for the higher cross-link densities in compression mode is unclear.

3.6. Thermal property

The DSC thermograms from −50 to 230 °C on lyophilized MPC polymer xerogel with different cross-linker are shown in Fig. 7. As a reference, HEMA polymer hydrogel cross-linked with 1 mol% of TEGDMA was synthesized. The bulk HEMA monomer was used for this reference and the synthetic method was the same as that of MPC polymer hydrogel. As for HEMA polymer hydrogel, the T_g was observed at 110 °C. This result well matches that of the HEMA polymer [28]. In the MPC polymer xerogels, however, no glass transitions were observed in this temperature range. That is, the thermal decomposition occurred before the glass transitions did. These results conclude that the T_g of MPC polymer chain is more than 230 °C and the MPC chain is more rigid than the HEMA polymer chain. The base line shifts around −20 °C were not T_g. These shifts were generated by the rapid cooling process by liquid nitrogen and they could not be reproduced (Fig. 8).

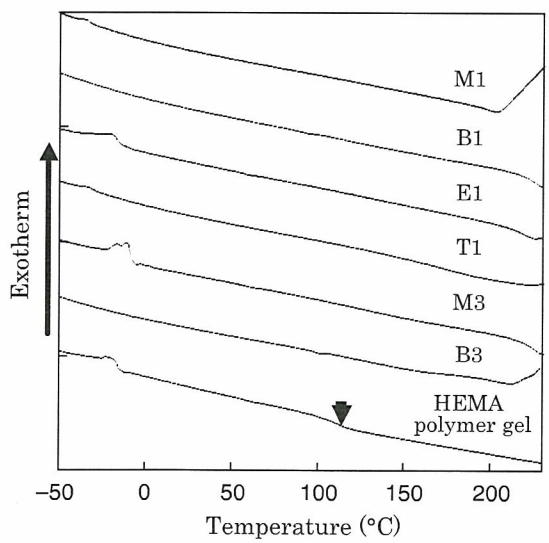

Fig. 8. DSC measurements of lyophilized MPC polymer hydrogels with various cross-linkers and concentrations in feed.

4. Conclusions

We synthesized MPC polymer hydrogels with a focus on the cross-linker to adjust the EWC and to enhance the mechanical properties for new ophthalmic materials, especially for SCL biomaterials. In addition, a novel water-soluble methacrylic cross-linker having a phosphorylcholine-like group, MMPC was applied to increase the free water content in the MPC polymer hydrogel. As a result, the free water content was slightly increased compared to a conventional hydrophilic cross-linker, BIS. We concluded that the phosphorylcholine-like group in MMPC increases the $W_{freezing}$ by loosely interacting with water molecules. The MMPC also enhanced the tensile properties with utilizing its hydrophilicity. In case of tensile tests, the fracture stress exceeded 120 kPa at M3, which had been considerably higher than for the conventional cross-linker. And, the MMPC was found to be higher reactivity in polymerization with MPC monomers than BIS. The novel cross-linker, MMPC, has a good potential for making soft biomaterials, particularly SCL.

Acknowledgements

The present research is supported in part by a Grant for the 21st Century COE Program 'Human-Friendly Materials Based on Chemistry' from the Ministry of Education, Culture, Sports, Science, and Technology of Japan.

References

[1] Okumura Y, Ito K. Adv Mater 2001;13(7):485–7.
[2] Griffith LG. Acta Mater 2000;48(1):263–77.
[3] Haraguchi K, Takehisa T. Adv Mater 2002;14(16):1120–4.
[4] Kopécek J. Eur J Pharmacol Sci 2003;20:1–16.
[5] Nicolson PC, Vogt J. Biomaterials 2001;22(24):3273–83.
[6] Smetana K, Vacík J, Souková D, Krová Z, Sulc J. J Biomed Mater Res 1990;24(4):463–70.
[7] Ishihara K, Ueda T, Nakabayashi N. Polym J 1990;22:355–60.
[8] Ishihara K, Nomura H, Mihara T, Kurita K, Iwasaki Y, Nakabayashi N. J Biomed Mater Res 1998;39:323–30.
[9] Ishihara K, Ziats NP, Tierney BP, Nakabayashi N, Anderson JM. J Biomed Mater Res 1991;25:1397–407.
[10] Ishihara K, Oshida H, Ueda T, Endo Y, Watanabe A, Nakabayashi N. J Biomed Mater Res 1992;26:1543–52.
[11] Ishihara K, Ishikawa E, Watanabe A, Iwasaki Y, Kurita K, Nakabayashi N. J Biomater Sci, Polym Ed 1999;10:1047–61.
[12] Sawada S, Sakaki S, Iwasaki Y, Nakabayashi N, Ishihara K. J Biomed Mater Res 2003;64A(3):411–6.